Thermo-Catalytic Conversion of Lignocellulosic Biomass to Distillate Fuels

by

Anthony Anderson

A dissertation submitted in partial fulfillment of the requirements
for the degree of

Doctor of Philosophy

(Chemical Engineering)

at the

UNIVERSITY OF WISCONSIN-MADISON

2022

Date of final oral examination: 12/09/2022

The dissertation is approved by the following members of the Final Oral Committee:

George W. Huber, Professor, Chemical and Biological Engineering

James A. Dumesic, Professor, Chemical and Biological Engineering

Ive Hermans, Professor, Chemical and Biological Engineering and Chemistry

Victor Zavala, Professor, Chemical and Biological Engineering

Siddarth Krishna, Assistant Professor, Chemical and Biological Engineering

Abstract

Catalytic activity tests were run to elucidate the chemistry and catalyst stability for the hydrodeoxygenation of aliphatic oxygenates over a $NiMoS_x/Al_2O_3$ catalyst at different pretreatments at hydropyrolysis conditions using glycerol as a thermally stable biomass model feedstock in a continuous flow reactor. Reactivity metrics were developed to quantify and compare the reactivity of NiMo for deoxygenation, hydrogenation, and C-C cleavage. Activity experiments showed sulfided NiMo and reduced NiMo catalysts had similar deoxygenation and hydrogenation activity for glycerol HDO at 400°C and 270 psig H_2 with the $NiMoS_x$ catalyst showing higher C-C cleavage activity. Without a sulfur co-feed, both the $NiMoS_x$ and $NiMoO_x$ catalysts lost >40% deoxygenation activity over 30 h time on stream. With a 2100 ppm H_2S co-feed the $NiMoS_x$ catalyst showed 12 times decrease in the deactivation rate for deoxygenation and 6 time decrease in the deactivation rate for hydrogenation. The main products at high conversion were propylene, propane, ethylene, methane, CO, methanol, ethanol, and 1-propanol. At low conversion, the major products were unsaturated allyl alcohol, acrolein, hydroxyacetone, and acetaldehyde. With no H_2S co-feed at short contact times, there was a significant amount of carbon loss due to condensation reactions, while at 2100 ppm H_2S in the feed, the carbon balance was 102.4%. Temperature programmed oxidation of the spent $NiMoS_x$ catalysts after 30 h of glycerol HDO without an H_2S co-feed showed that one of the causes of deactivation was coking.

An analytical semi-batch reactor was designed for the hydropyrolysis of maple wood, cellulose, and lignin. Heating rates of at-least 9.7°C/s were measured during hydropyrolysis experiments between temperatures of 200-400°C. Carbon balances between 86.3-88.9% were achieved for maple wood, lignin, and cellulose hydropyrolysis. Products in the range of C1-

C25 functionality were quantified utilizing FID, TCD, and MS techniques. FTICR-MS was utilized for analysis of heavy product functionality. Hydropyrolysis of cellulose produced mainly gasoline range products (38.5%) as n-paraffins, cycloparaffins, olefins, BTX, alcohols, and aldehydes as major products. Lignin hydropyrolysis produced mainly jet/diesel range products (36.0%) as paraffins, aromatics, polyaromatics, phenolics, olefins, and branched cycloparaffins. Whole biomass hydropyrolysis produced light gases (28.0%), gasoline range products (23.8%), and jet/diesel range products (10.6%) including all products seen from lignin and cellulose hydropyrolysis separately. Increasing the ratio of $NiMoS_x$ catalyst to biomass during hydropyrolysis from 5:1-20:1 increased overall yields and C-C bond cleavage for each cellulose, lignin, and whole biomass. FTICR-MS of lignin hydropyrolysis products show dimer species only while whole biomass hydropyrolysis products contained dimer and trimer species. The dimer and trimer species are mainly non-oxygenated or contain only one oxygen. Dimer and trimer species include hydrogenated species with only 2 DBE per monomer. Dimer species with a DBE ranging from 5-14 make up the major signal while unsaturated trimer species were not observed.

Acknowledgements

I am grateful to have attended and studied at the University of Wisconsin-Madison. These past 6 years have been arduous and obtaining a doctorate in Chemical and Biological Engineering would not have been possible without the assistance and patience from my professors, my family, and my peers. When I got a job in March 2021 in Texas, I could have never imagined I would be defending my thesis 21 months later. This journey has allowed me to grow in my professional life as an engineer and scientist as well as in my personal life.

I would like to thank my advisors Professor George Huber and Professor James Dumesic for their guidance, patience, and understanding through the past several years. I learned about their research during the summer of 2014 during my REU in Colorado and knew I wanted to learn from them one day. Professor Dumesic oversaw my research during my first year as a graduate student and through my repeated experimental speed bumps I learned the importance of documenting and learning from every experiment, especially the experiments that won't end up published. Professor Huber allowed me to pursue pyrolysis research through my hydropyrolysis project, the topic I was most interested in when I started my doctoral research. I learned how to plan my experiments based on hypothesis driven objectives and possible conclusions. I learned that experiments serve as a model for the scientific questions we have and that these models are only useful if you understand the experimental limitations. I learned how to be confident in my expertise while acknowledging my own limitations. I never imagined my first job out of graduate school would allow me to continue my passion for renewable chemicals and fuels, but for 21 months I have been a pilot plant engineer working

on developing biomass/plastic to renewable chemical technologies and I couldn't be happier about the fit.

I thank current and former group members in the Huber and Dumesic research groups for their instruction, discussion, and support. I would not have made it this far without the help of these scientists including Dr. Zach Brentzel, Dr. Ali Motagamwala, Dr. Mrunmayi Kumbhalkar, Dr. Dan McClelland, Dr. Kevin Barnett, Dr. Joseph Chada, Dr. Madelyn Ball, Dr. Nat Eagan, Dr. Juan Venegas, Dr. Peter Galebach, Dr. Theodore Walker, Dr. Keishla R. Rivera-Dones, Dr. Mark Lindsay, Dr. Jake Gold, Andrea Keane, Elise Gilcher, Dr. Alvin Jonathan, Dr. Paolo Cuello Penaloza, Leida M. Vazquez, Raka G. Dastidar, and Jiayang Wu. I also want to thank the undergraduate students that have collaborated with me on my projects over the years including Matthew Gargulak, Belma Sandoval, and Ben Davidson.

I would like to thank the faculty and staff in the Chemical Engineering department at UW Madison for their keen instruction and patience. I thank Professor Zavala, Professor Hermans, and Professor Krishna for being a part of my thesis committee. I am grateful for the assistance and understanding of Kate Fanis these past 21 months I've been in Texas.

I want to thank my collaborators at Exxon Mobil Research and Engineering including Dr. Michael Lanci, Dr. Kelsey McNeely, Dr. Chengrong Wang, Dr. Jillian Johnson, and Dr. Ashley Wittrig for their support and insight. My thesis research was possible, not only due to the funding provided by EMRE, but through the guidance, discussion, and critique from the brilliant scientists I worked with.

Most importantly, I would like to thank my wife Amanda Valleriano for her incredible patience and support. She made Wisconsin feel like my home and continues to provide the

comfort and security necessary for my success. Thanks to her, my lovely dog Wendy, and the endless support from my family, I was able to make it this far.

Table of Contents

List of Figures and Tables

1. Introduction

1.1.Fuels from the thermochemical conversion of lignocellulosic biomass

Lignocellulosic biomass is a cheap and abundant source of carbon that may be converted through thermochemical processes to produce renewable fuels.[1] Due to the growing demand of jet and diesel fuels, it is desired to produce these fuels from lignoceullosic biomass since they could potentially directly replace fossil fuels for this application.[2] The energy density of carbon-based liquid fuels also serves as a key advantage over batteries for electric vehicles.[3-4]

Lignocellulosic biomass is composed of three major biopolymer components: Lignin, Cellulose, and Hemicellulose.[5-6] Cellulose is the most abundant component and has been commonly utilized through the production of cellulosic ethanol via biochemical processes.[7-8] Hemicellulose is composed of C5 and C6 monomers with a range of compositions, varying depending on the type of biomass. Lignin is composed of propylphenol based subunits with various linkages connected through C-C and ether bonds. The B-O-4 bond, an ether linkage, is the most common-linkage and easily cleaved through thermal or catalytic pathways. Other C-C bond linkages are difficult to selectively cleave. An example of the lignin structure containing various bond types can be seen in Figure 1.1

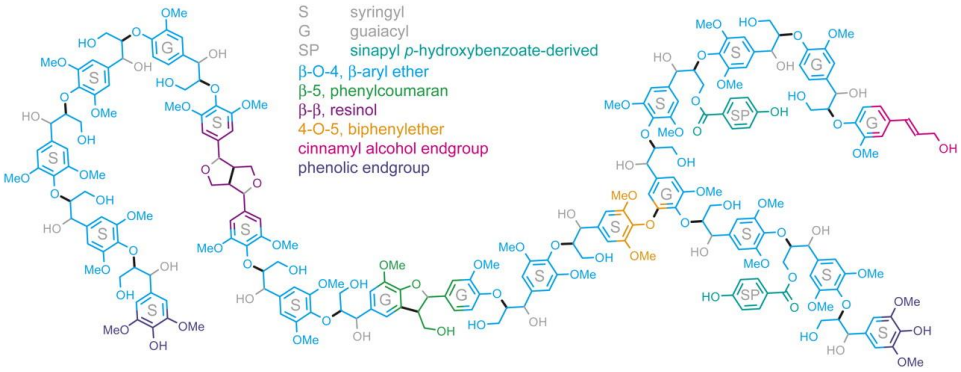

Figure 1.1 Example of lignin polymer from poplar lignin shown by Stewart, et al. [9]

1.2. Biomass Pyrolysis

Fast pyrolysis is a process in which lignocellulosic biomass is rapidly heated and thermally depolymerized to form bio-oil. Efficient utilization of the bio-oil is challenging as the poor fuel characteristics such as low-energy density (16-22MJ/kg), high water content, and high acidity (pH<3) hinder its use in most liquid-fuel applications.[9-10] The produced bio-oil is also immiscible with conventional petroleum feedstocks and is unstable, polymerizing during storage.[6,11] Catalytic fast pyrolysis utilizing zeolites can produce olefins and aromatics such as benzene, toluene, xylenes, and naphthalenes.[12] [13] This allows for selective C-C coupling of olefins to BTX while the majority of the oxygen is removed through decarbonylation.[12,14-16] Catalytic hydrodeoxygenation has been proposed as a technology to remove the oxygen content and increase the fuel value of bio-oil using traditional hydrotreating sulfide NiMo and CoMo catalysts.[11-12,17-21] However, these catalysts often deactivate by several proposed mechanisms including coking, mineral deposition, phase change, and leaching.[22-24] Fast pyrolysis of biomass produces hundreds of different compounds including organic acids, alcohols, furans, and large phenolic oligomers.[25] Hydrotreating of pyrolysis oils produces hundreds of different hydrocarbons alkanes from C_1 to C_{24}.[11]

1.3. Biomass Hydropyrolysis

A biomass conversion technology that is similar to fast pyrolysis called Hydropyrolysis has been proposed by Pindoria et al. and Marker et al.[26-27] Hydropyrolysis involves pyrolyzing the biomass in the presence of hydrogen gas using NiMo and CoMo catalysts. Marker et al. reported that the Integrated Hydropyrolysis and Hydroconversion (IH^2) was able to obtain yields up to 26 wt% C4+ on the 50 kg/day scale from maple wood biomass.[27-28] This technology now is being commercialized by Shell and Criterion.[29] In this process, lignocellulosic biomass is pyrolyzed in a fluidized bed reactor in the presence of a sulfided, molybdenum based hydrotreatment catalyst followed by hydrotreatment in a secondary packed bed reactor. Figure 1-2 shows a simplified representation of the hydropyrolysis process. The first step of hydropyrolysis is the thermal pyrolysis of biomass. Hydrodeoxygenation, decarbonylation, decarboxylation, and hydrogenation allows for most of the oxygen to be removed before the reactive vapors are allowed to oligomerize, effectively stabilizing the pyrolysis intermediates. The light gases produced in this reaction are reformed for both heat and the required hydrogen. Marker et al. has reported that the sulfided catalyst remained stable for 750 h ToS, with no information regarding a sulfur co-feed or any continuous regeneration.[27-28,30]

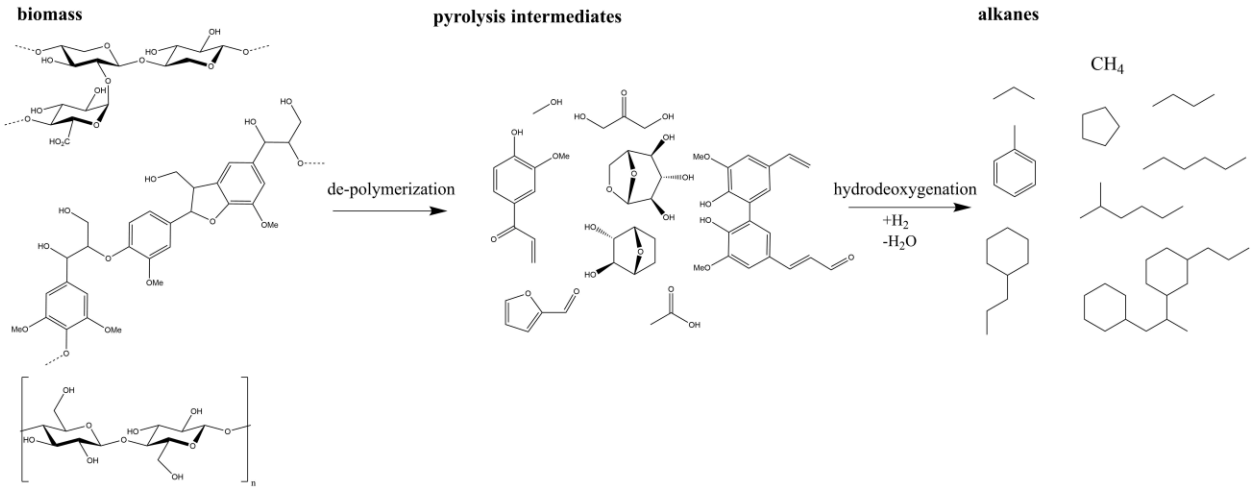

Figure 1.1: The overall process for the hydropyrolysis of lignocellulosic biomass, displaying the thermal depolymerization of biomass followed by the subsequent hydrodeoxygenation of resulting vapors.

Several other groups have published studies on the hydropyrolysis of lignocellulosic biomass in fluidized bed reactors using molybdenum based hydrotreatment catalysts.[31-34] Dayton et al. tested the hydropyrolysis of loblolly pine with a reduced $NiMo/Al_2O_3$ catalyst showing non-aqueous C_4+ yields as high as 24.1 wt% with an oxygen and moisture content of 2.4 and 2.5 wt% respectively. The catalyst stability was tested by 10 sequential 90 min experiments followed by oxidation and reduction after each, showing no major change in yield over these 10 experiments, yielding an average organic yield of 22.5 ± 1.35 wt% with an oxygen content of 2.8 ± 0.99 wt%.[31] Stummann et al. tested the hydropyrolysis of beech wood with a sulfided $NiMo/MgAl_2O_3$ and $CoMo/MgAl_2O_3$ catalysts at 450°C and 26bar, with C_4+ organic yields varying between 24.3 and 26.4 wt% with an oxygen content of between 9.0 and 12 wt% on a dry basis. The stability of the catalysts were not explicitly tested, but the carbon content on the catalysts ranged from 0.9 and 3.3 wt% with 2.4 wt% potassium on the surface of the catalyst.[33] These empirical studies have shown the promise of sulfided Mo catalysts

for conversion of biomass, yet few have reported fundamental studies on the hydrodeoxygenation of biomass with these catalysts.

1.4. Molybdenum Based Hydrotreatment Catalysts

Density functional theory (DFT) studies by Kasiraju et al. have shown hydrodeoxygenation (HDO) over a MoO_3 catalyst and hydrodesulphurization (HDS) over a MoS_2 catalyst follow similar mechanisms.[35] It has been proposed that the active site of a molybdenum based hydrotreatment catalyst is the vacancy of sulfur atoms on the surface, with nickel or cobalt atoms promoting the activity of these catalysts by forming bridge sites between the molybdenum and promoter atom at the edge.[36] A Sulphur vacancy in the MoS_2 phase is active for heteroatom removal, but is stabilized and promoted by nickel or cobalt edge sites.[37-39] The main difference between the HDO and HDS mechanisms is the removal of the remaining sulfur or oxygen by hydrogen.[35] Upon sulfiding, acid sites in the form of sulfhydryl groups can also form. Sulfur co-feeds such as H_2S, dimethyldisulfide (DMDS), dimethylsulfoxide (DMSO), or other liquid sulfiding agents are required during HDO to prevent removal of sulfur from the surface.[37,40]

Model oxygenate studies show promising stability during HDO when sulfur is co-fed, but these studies have typically been carried out at bio-oil hydrotreatment conditions (300°C and 200bar) using oxygenate models with different effective carbon/hydrogen ratios than pyrolysis vapors.[41-46] The effective carbon/hydrogen ratio is used to describe the difficulty of upgrading a feedstock through hydrotreatment and takes into account the required hydrogen for hydrodeoxygenation.[15,46] Dabros et al. carried out HDO of ethylene glycol over $NiMoS_x$, $CoMoS_x$, and MoS_x catalysts supported on $MgAl_2O_3$ at 400°C and 27 bar H_2, showing over

35% reduced conversion after 70 h TOS with a 550 ppm H_2S co-feed. The stability of each catalyst was improved by increasing the H_2S co-feed from 550 to 2200 ppm. The catalysts also showed C-C bond cleavage with C_2/C_1 ratios ranging from 1.5-4.8. Through XAS studies, the stability promotion was attributed to less exchange of the oxygen and sulfur on the surface with higher partial pressure of H_2S and the use of Ni and Co promoters.[37] Biomass hydropyrolysis consists of many sequential and parallel C-C cleavage, hydrogenation, deoxygenation, and C-C coupling steps. Saturated products are formed during this process by hydrotreatment, deoxygenation and hydrogenation with lighter products formed by C-C bond cleavage. Limited work has been done on the hydrodeoxygenation of simple, chemically similar model compounds of lignocellulosic biomass at hydropyrolysis conditions.

1.5. Hydropyrolysis Reactor Design

At the industrial scale catalytic fluidized bed technologies are ideal for hydropyrolysis due to scalability, heat/mass transfer, and continuous regeneration. Biomass pyrolysis results in high coke yields, requiring continuous regeneration of the catalyst. Zeolite catalysts are utilized for catalytic fast pyrolysis technologies (CFP) for the conversion of biomass to distillate fuels and commodity chemicals such as BTX.[15,47] Hydropyrolysis requires hydrogenation metals for hydrogenolysis to limit yields of CO_x and maximize yields of distillate ranged hydrocarbons.[26,48] Continuous regeneration of coked precious metal catalysts requires both coke burning and reduction steps. Similarly, hydropyrolysis utilizing sulfided molybdenum-based catalysts requires continuous sulfiding following coke oxidation. Due to the high partial pressures of Hydrogen required and the low density of Hydrogen, hydropyrolysis typically

requires total pressures of >20bar.[49-51] This process is challenging to mimic effectively at the laboratory scale due to solids handling and transport effects.[52-53] To effectively model hydropyrolysis conditions, laboratory reactors must operate within similar Hydrogen and reactant partial pressures, fast feedstock heating rates (>10°C/s), and low gas residence times(< 5s). Hydropyrolysis of biomass in fluidized bed reactors at the laboratory scale has been studied by Stumman Et al. and Dayton Et al..[31-34,49,54-56] They are able to achieve oxygen free oil yields up to 25 wt% utilizing a fluidized bed reactor and a downstream hydrodeoxygenation fixed bed with molybdenum-sulfide based catalysts.[57] A secondary hydrotreatment bed has been proposed to minimize oxygen in the product while limiting catalyst deactivation, especially from mineral deposition.[27-28,48,54] Batch hydropyrolysis is often non-representative due to long gas residence times, poor catalyst contact, low pressures, or low heating rates.[51,58-59] The Pyroprobe technology is utilized to study pyrolysis chemistry, but often has poor catalyst/biomass contact, low pressure operation, and a low carbon balance.[58] This technology utilizes a resistivity heated coil to heat a microgram quantity sample of biomass while gas flows over the pyrolysis cell. The resultant vapors are then passed through a catalyst bed and either injected directly into an MS or collected in a cold trap and injected in an MS after the experiment. Venkatesan Et al. studied the hydropyrolysis of pine wood at varying pressures within a Pyroprobe fit with a stainless-steel reactor bed, noting an increase in oxygen removal and hydrocarbon yield at 20 bar H_2 and 500°C compared to 1 bar. Most Pyroprobe studies are only semi-quantitative, mostly focusing on product identification. Overall carbon yields are typically 20-50% with as high as 85% being reported in studies where appropriate heat tracing and direct GC-MS injection are utilized.[12,14,47,60-62]

1.6. Scope

In chapter 2, the objective of this work was to measure the reactions rates of deoxygenation, C-C bond cleavage, and hydrogenation for HDO of glycerol over reduced and sulfided NiMo/Al_2O_3 catalysts in a continuous flow reactor. During glycerol HDO oxygen is removed and hydrogen is added forming a variety of deoxygenated products as shown in Figure 1.2. These intermediates are similar to the products found during cellulose pyrolysis, making glycerol a good model for the cellulose and hemicellulose portion of biomass. The glycerol HDO reaction network only contains 20-30 common products enabling sufficient identification and quantification of each product. Generally, reaction rates and deactivation are studied at low conversion to allow for a relatively constant partial pressure of reactant for kinetic measurements. For reaction networks containing several reaction types in series and parallel with thermally unstable reactants and intermediates, low conversion experiments are not possible. A method for measuring the extent of deoxygenation, hydrogenation, and CC cleavage was developed to quantify the three major reaction types during the HDO of glycerol. This allows for a semi-quantitative method to measure activity of the catalyst across these reaction types for a complicated reaction network with dozens of products at 100% conversion of feed. The stability and activity of reduced and sulfided NiMo/Al_2O_3 catalysts were compared. While the stability of sulfided Mo-based catalysts have been investigated for hydrodeoxygenation in other studies, this has typically been limited to simple deoxygenation reactions. Due to the similar functionality of glycerol to the cellulose and hemicellulose fractions of biomass, glycerol HDO may show similar deactivation pathways for of sulfided NiMo catalysts. Since glycerol HDO does not include polyaromatic oxygenates or mineral

impurities, some potential deactivation mechanisms may not be assessed through this study. A catalyst stability study through biomass hydropyrolysis experiments is more challenging operationally and analytically due to the continuous run-time requirement and detailed reaction network elucidation.

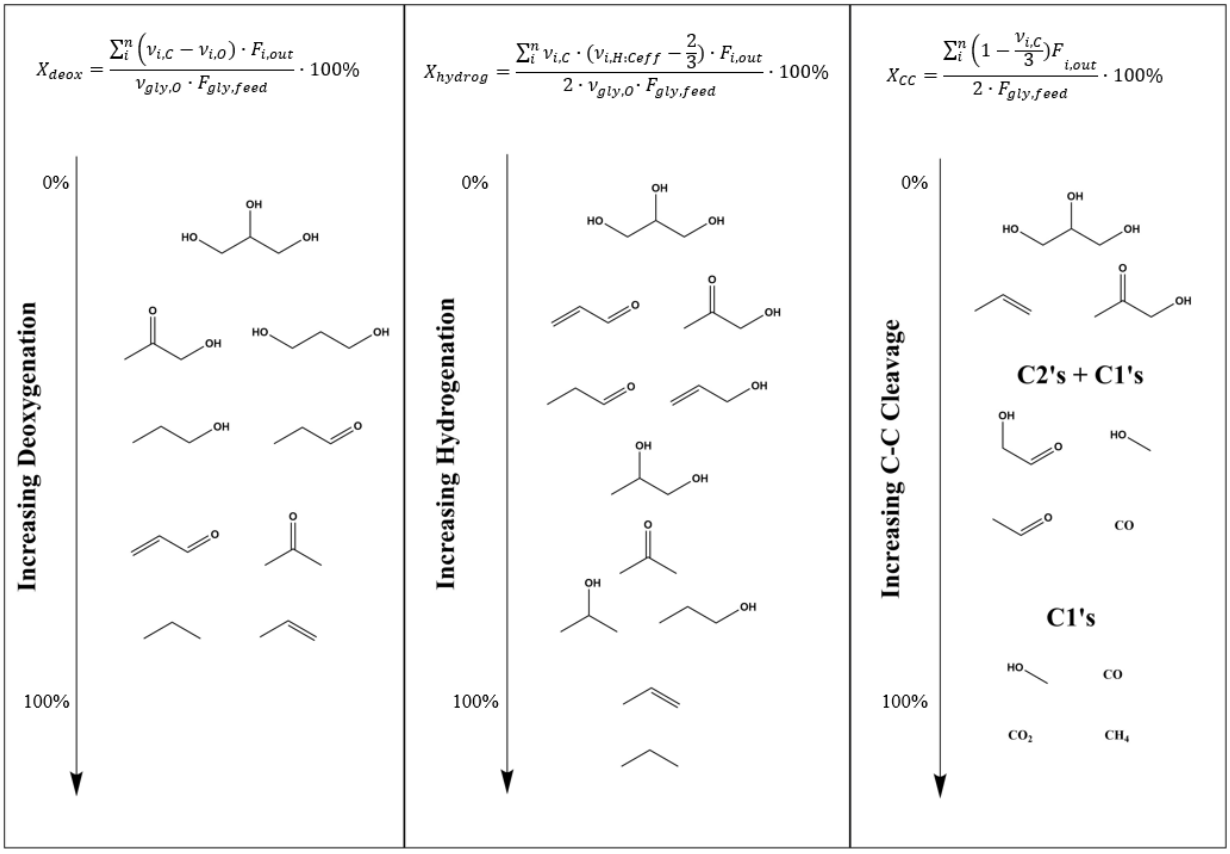

Figure 1.2: The overall process for the hydropyrolysis of lignocellulosic biomass, displaying the thermal depolymerization of biomass followed by the subsequent hydrodeoxygenation of resulting vapors.

In chapter 3, the hydropyrolysis of maple wood over sulfided $NiMo/Al_2O_3$ is conducted in a novel laboratory scale reactor. This reactor was designed to closely match key process conditions of hydropyrolysis within a fluidized bed reactor while remaining versatile and high throughput. Heating rate, reaction temperature, H_2 partial pressure, oxygenate partial pressure,

and gas residence times all significantly affect the products formed through hydropyrolysis. Testing varying catalyst:biomass ratios during the semi-batch hydropyrolysis of biomass allows for reaction network elucidation. At low catalyst:biomass ratios (1:1-5:1), the pyrolysis vapors are only partially hydrodeoxygenated. Analysis of these intermediates is challenging considering their stability and high boiling point. This typically results in a low carbon balance due to the formation of heavy oligomers, coke, and secondary char. These results can still be useful, since it is generally understood that the missing carbon is mainly unobserved and unmeasured heavy oligomers. Varying the catalyst:biomass ratio for a semi-batch reaction is experimentally analogous to varying contact time for a continuous fixed bed reactor. Thus, an increase in catalyst:biomass ratio will result in more catalytic reactions for hydrogenation, C-C cleavage, and deoxygenation. This limits the homogeneous reactions between reactive intermediates, improving overall observable yields. The hydropyrolysis of maple wood, cellulose, and maple lignin are investigated to better understand the products from each major lignocellulosic biomass fraction during hydropyrolysis.

2. Glycerol HDO

The work done on glycerol HDO has been previously published in ChemCatChem.[63]

2.1. Experimental

2.1.1. Catalyst preparation

A low NiMo catalyst supported on γ-alumina from Albemarle Catalyst Company was received in the oxide state and was used in either a reduced or sulfided state. The $NiMoO_x$ catalyst was reduced under H_2 flow at 270 psi and ramped at 1°C min^{-1} to the 400°C reaction temperature prior to reaction. The $NiMoS_x$ catalyst was sulfided as instructed by the catalyst vendor. The catalyst was pretreated in batches in a H_2S/H_2 atmosphere by flowing 4 wt% dimethyl disulfide (DMDS) in heptane with an Eldex Optos Model 1 piston pump at a WHSV of 2 h^{-1} and H_2 gas at a GHSV of 600 h^{-1} while carefully ramping the temperature as shown in Figure 2.1. Afterwards, the catalyst was cooled under argon flow to room temperature where the sulfided catalyst was passivated with air before removing from the reactor. Prior to every experiment with $NiMoS_x$, the passivated catalyst was heated at 1°C min^{-1} and held at 400°C for 1 h with 4 wt% DMDS in heptane pumped at a WHSV of >2 h^{-1} and H_2 gas at a GHSV of at least 600 h^{-1}.

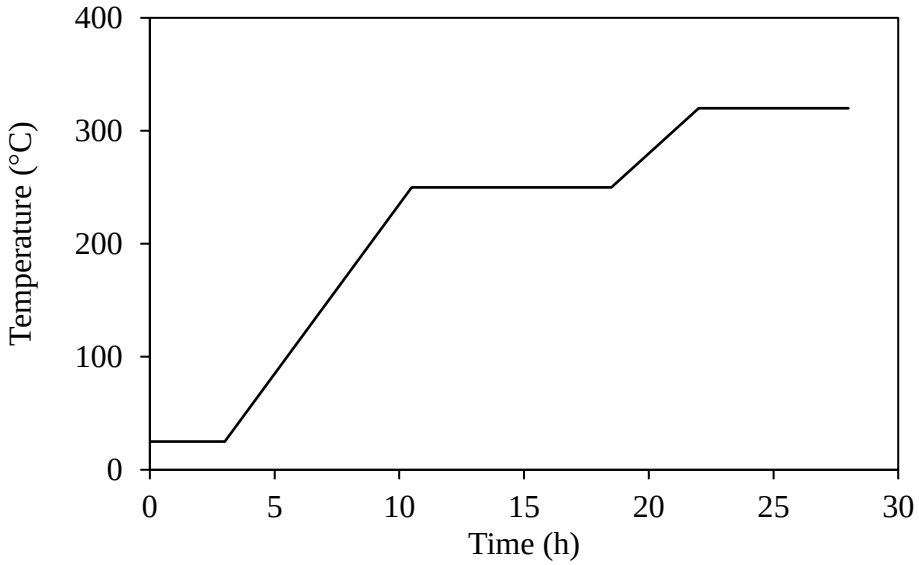

Figure 2.1: Reactor temperature over time during the sulfiding pre-treatment of the NiMoOx catalyst.

2.1.2. Catalyst characterization

The spent catalysts were characterized via temperature-programmed oxidation (TPO) using a Micrometrics AutoChem II 2920 instrument equipped with a Cirrus 2 Quadrupole Mass Spectrometer. During TPO, 50 mg of catalyst was loaded into a quartz u-tube and dried for 2 h at 150°C with 50 mL min^{-1} He flow. After cooling to room temperature, the sample was heated at a rate of 10°C min^{-1} to 700°C with 50 mL min^{-1} of 10% O_2 in He. The CO_2, CO, and SO_2 were detected using mass spectrometry. The CO_2 and CO were calibrated to quantify the carbon from oxidation through integration. The surface area before and after reaction was determined by the Brunauer-Emmett-Teller (BET) method using a Micrometrics ASAP 2020 Plus instrument.

2.1.3. Experimental setup

A fixed bed reactor was used to conduct gas phase glycerol hydrodeoxygenation (HDO) as shown in 2-2. Reactors were made with ¼" in diameter and 0.014" wall thickness 316L stainless steel tubing. For a typical reaction, 130 mg of catalyst was placed in the middle of a 10" long reactor between quartz wool and silica chips. The contact time (reported in seconds) of the glycerol reactant flowrate (g_{feed} s^{-1}) over the NiMo catalyst (g_{cat}) was varied by changing the catalyst amount. For experiments at a contact time of 3 s, the catalyst was diluted 50 times with 40-60 mesh crushed silica. The contact time was varied by changing the amount of added catalyst. Experiments with < 100 mg of catalyst used catalyst diluted with silica chips ground and sieved to the same particle size as the $NiMoS_x/Al_2O_3$. A glycerol HDO experiment with only silica chips was run and showed a carbon balance of 98.6% with no observed products. The catalyst was pretreated prior to the run according to the conditions in the catalyst preparation section. Once reaction conditions were met, the reaction was started by pumping 80% glycerol in water via an Eldex Optos Model 1 piston pump and flowing a mixture of ultrahigh purity (UHP) grade H_2 (Airgas) and 2% H_2S in H_2 (Airgas). Liquid samples were collected from a pressurized collection vessel cooled to 0°C about every 2 h after the start of a reaction. The first liquid sample is transient and is not analyzed. The gas stream was sampled every 2 h, before every liquid sample. The spent catalyst was cooled to ambient temperature, purged with ultrahigh purity (UHP) grade Argon (Airgas) and passivated with air by flowing ultrahigh purity (UHP) grade air (Airgas) at 50 mL min^{-1} for 30 min prior to removal from the reactor. The partial pressures, temperature and contact times used in this study are shown in Table 2.1.

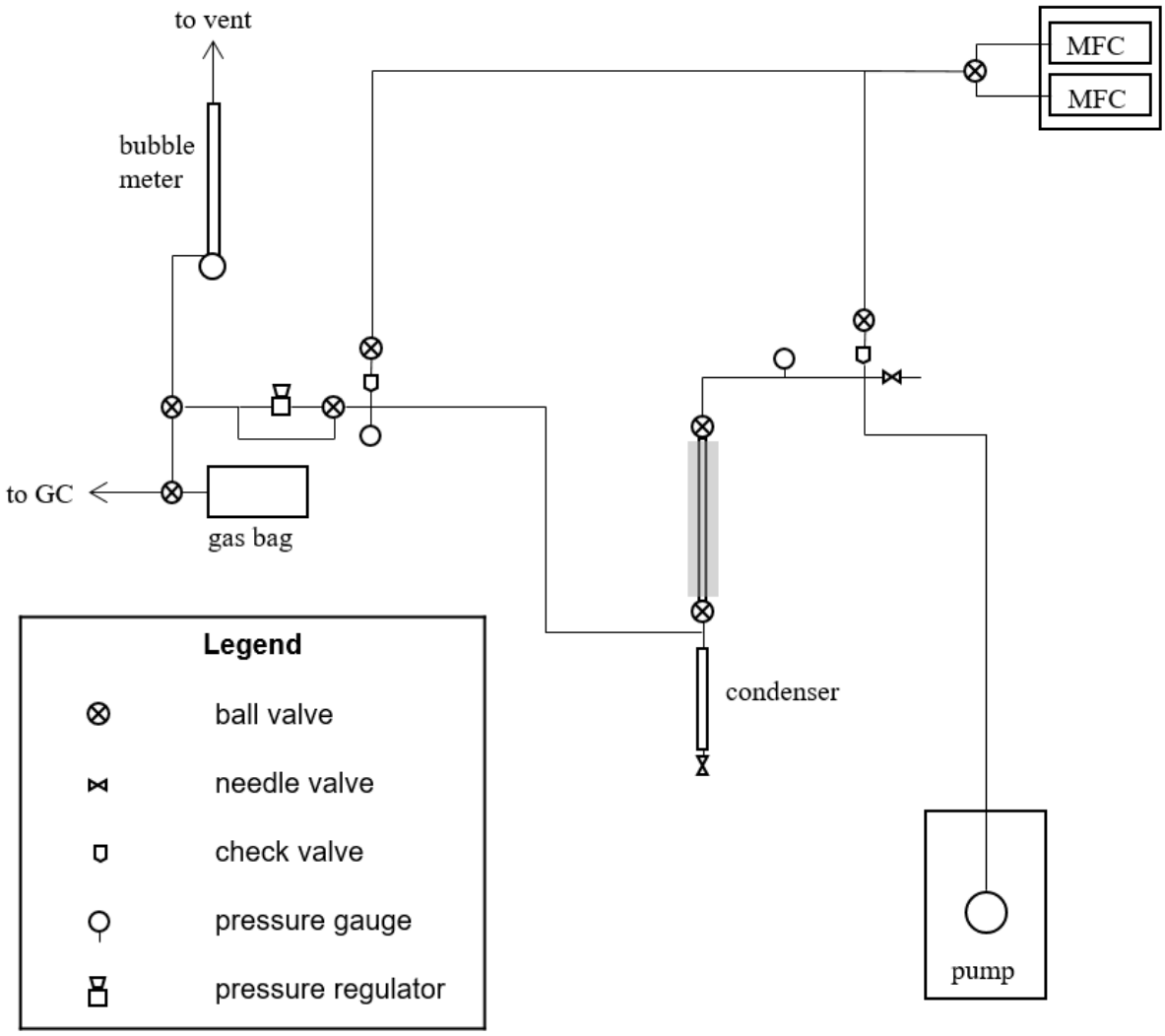

Figure 2.2: A simplified schematic of the packed bed flow reactor used for the continuously fed hydrodeoxygenation of glycerol at hydropyrolysis conditions.

Most hydrodeoxygenation studies operate around 300°C at varying partial pressures of hydrogen ranging from atmospheric to 2000 psi. Hydropyrolysis must be run >400°C for fast pyrolysis to occur. Due to capital costs, operational costs, and operational safety, it is desirable to limit the operating pressure of fluidized bed reactors. The process conditions for

HDO of glycerol are shown in Table 1. Operating within similar temperatures, partial pressures, and gas residence times is critical for obtaining results relevant to larger scale fluidized bed reactor technologies.[27,64]

Table 2.1: The process conditions for the hydrodeoxygenation (HDO) of glycerol at hydropyrolysis conditions.

Process Condition	
Temperature (°C)	400
Pressure (psig)	270
Hydrogen pressure (psi)	250-263
Water pressure (psi)	3-13
H_2S pressure (psi)	0.0-0.6
Glycerol pressure (psi)	3
Gas residence time (s)	1

2.1.4. Product analysis

Gas samples were analyzed by an online Shimadzu GC-2014 instrument equipped with a sample loop and both a thermal conductivity detector (TCD) and flame ionization detector (FID). The TCD detector was used to quantify CO and CO_2 while the FID detector was used to quantify C1-C3 hydrocarbons and oxygenates. Permanent gases were identified and calibrated with triplicate single point calibration using SCOTTY specialty gas mixtures. Volatile oxygenates were identified by gas bag injection and quantified using the effective carbon number (ECN) and their respective carbon number alkane. samples were diluted by 8

times in water and by 5 times in tetrahydrofuran (THF) before analysis.[65] Liquid samples were identified using a Shimadzu GC-2010 instrument with a RTX-VMS column equipped with a Shimadzu GCMS-QP2010 mass spectrometer and quantified using a Shimadzu GC-2010 instrument equipped with a FID and RTX-VMS column.

The conversion of glycerol, X_{gly}, was calculated according to Equation 1 where $F_{gly,feed}$ is the molar flow rate of glycerol into the reactor and $F_{gly,prod}$ is the molar flow rate of glycerol out of the reactor . The carbon yield of any product i, Y_i, is described in Equation 2 where $\nu_{i,C}$ is the number of carbon atoms in product i and $F_{i,out}$ is the molar flow rate of product i. The carbon balance, Y_{CBal} is described in Equation 3 which is calculated based on the total carbon fed into the system as glycerol and the gas and liquid products measured by GC-FID, where n, is the total number of products. We have introduced a variety of other conversions to analyze the complex products that are occurring in this reaction. The deoxygenation conversion, X_{deox}, is described in Equation 4 and is a molar conversion of C-O bonds cleaved in glycerol based on the observed gas and liquid products where $\nu_{i,O}$ is the number of oxygen atoms in the product. The deoxygenation metric ranges from 0 to 100%, where 100% deoxygenation would indicate that 100% of the C-O bonds in glycerol were cleaved, resulting in a carbon yield of 100% alkane/alkene products. The hydrogenation conversion, X_{hydrog}, is described in Equation 5 and is a molar conversion of hydrogenations based on the amount of hydrogen in the observed gas and liquid products and the number hydrogenation events required to convert glycerol to propane. $\nu_{i,H}$ is the number hydrogen atoms in product i and $\nu_{gly,H}$ is the number of hydrogen atoms in glycerol. This metric ranges from 0 to 166.6 %, where 100% hydrogenation conversion indicates glycerol being converted

to water and propane, and 166.6% hydrogenation indicates glycerol being converted to water and methane. The C-C cleavage conversion, X_{CC}, is described in Equation 6 which is a molar conversion of C-C bonds in glycerol based on the observed gas and liquid products. This metric ranged from 0 to 100%, where 100% C-C cleavage conversion indicates 100% of the C-C bonds in glycerol were cleaved to form all C1 products.

$$X_{gly} = \frac{F_{gly,feed} - F_{gly,prod}}{F_{gly,feed}} \cdot 100\% \quad (1)$$

$$Y_i = \frac{\nu_{i,C} \cdot F_{i,out}}{3 \cdot F_{gly,feed}} \cdot 100\% \quad (2)$$

$$Y_{CBal} = \frac{\sum_i^n \nu_{i,C} \cdot F_{i,out}}{3 \cdot F_{gly,feed}} \cdot 100\% \quad (3)$$

$$X_{deox} = \frac{\sum_i^n (\nu_{i,C} - \nu_{i,O}) \cdot F_{i,out}}{3 \cdot F_{gly,feed}} \cdot 100\% \quad (4)$$

$$X_{hydrog} = \frac{\sum_i^n 0.5 \cdot \nu_{i,C} \cdot (\nu_{i,H:Ceff} - \frac{2}{3}) \cdot F_{i,out}}{3 \cdot F_{gly,feed}} \cdot 100\% \quad (5)$$

$$X_{CC} = \frac{\sum_i^n (1 - \frac{\nu_{i,C}}{3}) F_{i,out}}{2 \cdot F_{gly,feed}} \cdot 100\% \quad (6)$$

The rate of deactivation was approximated with first order deactivation kinetics, described by Equation 7, where $\beta_{1,j}$ is the first order deactivation constant and a_j is the conversion at time, t, relative to the initial conversion. j denotes the type of activity: deoxygenation, hydrogenation, or C-C cleavage.

$$\ln(a_j) = -\beta_{1,j} t \qquad (7)$$

Three metrics for these various reaction types were developed to compare catalyst activity for glycerol HDO including the deoxygenation conversion, hydrogenation conversion and the C-C bond cleavage conversion. These metrics are a part of a novel analysis method which can be applied to other studies with complicated networks with various reactions occurring in series and in parallel. Glycerol was chosen as the feedstock because it is thermally stable unlike pyrolysis oil or pyrolysis vapors. Glycerol has previously been used as a model to study the aqueous phase reforming of sugars and sugar alcohols.[66] This work seeks to identify the role of sulfur on catalyst stability for hydrotreating catalysts and the mechanism of catalyst deactivation during HDO at hydropyrolysis conditions in a continuous flow reactor.

2.2. Results and Discussion

2.2.1. Glycerol HDO over $NiMoS_x$ and $NiMoO_x$ catalysts with varying H_2S co-feeds

Figure 2.3 shows deoxygenation, hydrogenation, and C-C cleavage conversions along with the product yields with time on stream for glycerol HDO over $NiMoO_x$ with no H_2S in the feed. The products are divided into three main categories: alkanes/alkenes, oxygenates, and CO_x. The alkanes/alkenes consist of propane, propylene, ethane, ethylene, and methane. The oxygenates consist mainly of 1-propanol, allyl alcohol, propionaldehyde, acrolein, hydroxyacetone, acetaldehyde, ethanol, and methanol. The CO to CO_2 ratio is about 4:1. At 3.3 h TOS, the deoxygenation, hydrogenation, and C-C cleavage conversion are 82.5%, 62.9%, and 11.8% respectively. After 29.9 hours time on stream (TOS) these conversions all decrease to 43.1%, 18.7%, and 8.9% respectively. The initial products are highly deoxygenated and saturated compounds such as propane, propylene, and mono-alcohols demonstrating that $NiMoO_x$ is an active catalytic material for deactivation. As the catalyst deactivates, the extent of deoxygenation and hydrogenation is reduced and the major products are oxygenated compounds such as propionaldehyde, hydroxyacetone, and acrolein (Figure 2.3).

Figure 2.4 shows deoxygenation, hydrogenation, and C-C cleavage conversions along with the product yields with time on stream for glycerol HDO over $NiMoS_x$ with no H_2S in the feed. At 3.3 h TOS, the deoxygenation and hydrogenation conversions are 70.2% and 42.3% respectively, lower than the values for HDO of glycerol over $NiMoO_x$ at the same conditions. The deoxygenation and hydrogenation conversions decrease to 39.3% and 12.3% respectively after 28.7 h TOS. The initial C-C cleavage conversion is higher for $NiMoS_x$ at 28.0% than $NiMoO_x$ at 11.8%. All products observed for glycerol HDO over $NiMoS_x$ are observed while

using $NiMoO_x$. The major difference between these two catalysts is the C-C cleavage activity, where $NiMoO_x$ produces 3.0% CO_x initially while the $NiMoS_x$ produces 18.9% CO_x. Regeneration of the $NiMoS_x$ catalyst was attempted by calcination up to 500°C and sulfiding following the procedure described previously. After deactivating to 62.2% of the initial deoxygenation activity, only 82.2% of the initial activity was returned after the first regeneration and the catalyst continued to deactivate quickly. A second regeneration resulted in only 63.1% of the initial deoxygenation activity.

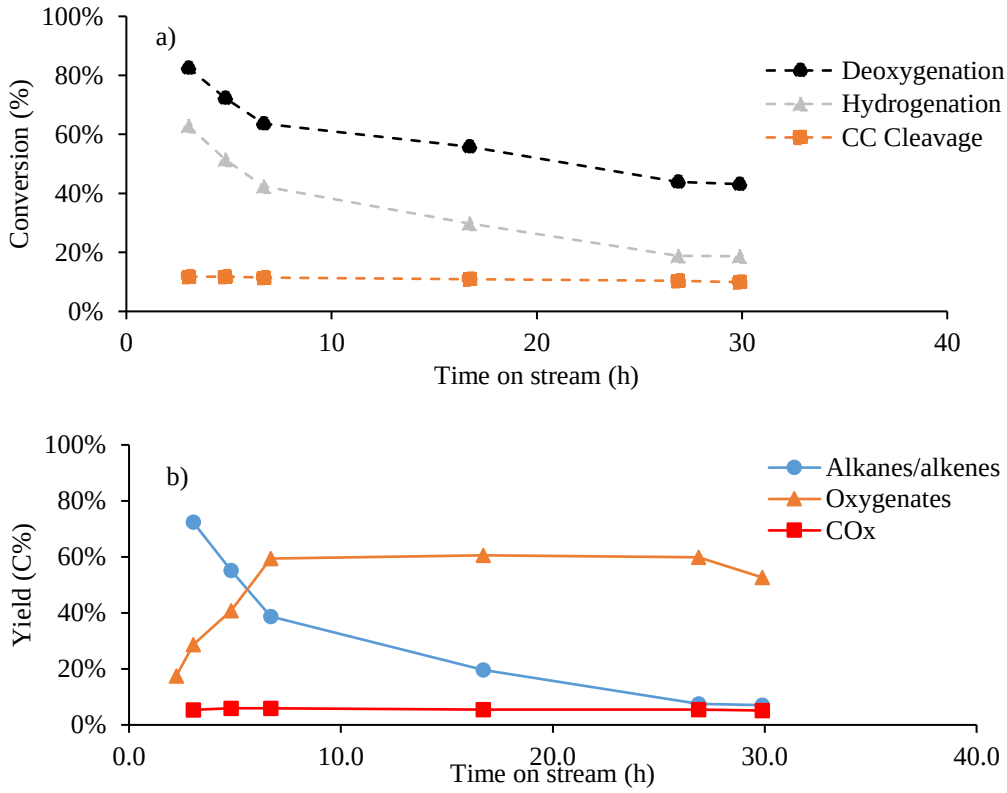

Figure 2.3: Glycerol HDO over NiMoOx catalyst with no sulfur co-feed. Reaction conditions: 400°C, 270 psig, contact time of 360 s.

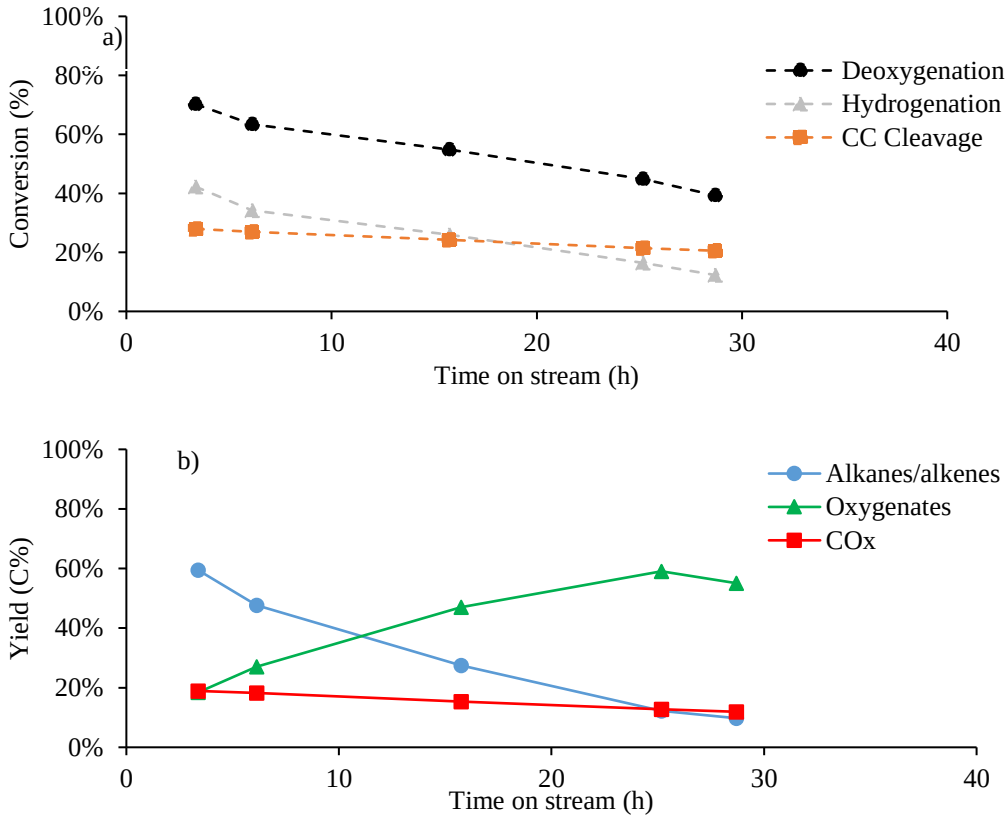

Figure 2.4: Glycerol HDO over NiMoSx catalyst with no sulfur co-feed. Reaction conditions: 400°C, 270 psig, contact time of 360 s.

Hydrogen sulfide gas was introduced in the reaction feed by co-feeding a gas stream of 2% H_2S in H_2. The first data points for these experiments were taken at about 3 h TOS, shown in Figure 2.5. The products when H_2S was co-fed with the hydrogen were the same as the products without an H_2S co-feed. At 3.0 h TOS, the deoxygenation and hydrogenation conversions are 82.7% and 72.5% respectively with a 2100 ppm H_2S co-feed. This is a similar activity for glycerol HDO with $NiMoS_x$ catalyst without an H_2S co-feed. After 30.1h TOS the deoxygenation and hydrogenation decrease to 78.1% and 57.9% respectively. The initial C-C cleavage conversion is 22.3%, lower than the 28.0% observed with no H_2S co-feed. The C-C cleavage increases from 22.3% to 30.7% after 30.1 h TOS.

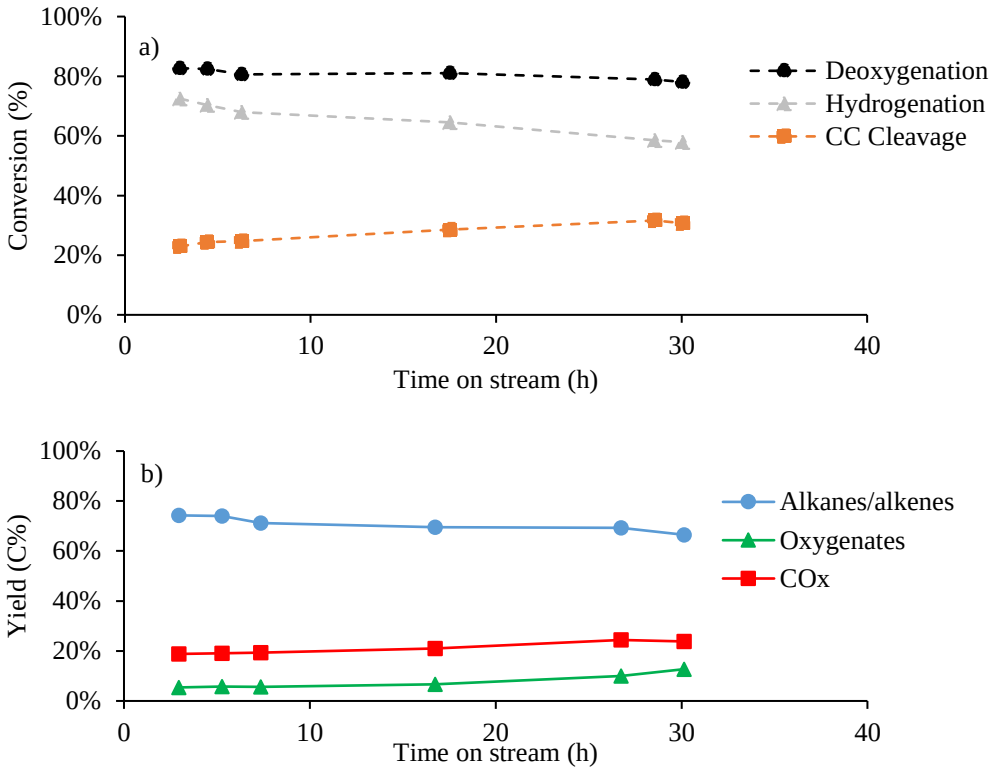

Figure 2.5: Glycerol HDO over NiMoSx catalyst with 2100 ppm H2S co-feed feed. Reaction conditions: 400°C, 270 psig, contact time of 360 sg¬cat/gfeed.

Table 2.2 shows the conversions, deactivation rate constants, and carbon yields for $NiMoO_x$ and $NiMoS_x$ with varying H_2S co-feeds. Without a sulfur co-feed, the deactivation rate constants for deoxygenation and hydrogenation for $NiMoS_x$ and $NiMoO_x$ are similar. However, $NiMoS_x$ has a higher deactivation rate constant for C-C cleavage than $NiMoO_x$. When 2100 ppm H_2S is added to the feed for $NiMoS_x$ catalyst the deoxygenation and hydrogenation deactivation rate constants reduce from 2.12E-2 and 4.50E-2 h^{-1} (without H_2S) to 0.17E-2 and 0.76E-2 h^{-1} (with H_2S) respectively. Also shown in Table 2.2 is the activity of a $NiMoS_x$ for glycerol HDO with 700 ppm H_2S in the feed. The deactivation rate constants for deoxygenation and hydrogenation were 0.13E-2 and 1.26E-2 $h^{-1,}$ respectively. This shows only a moderate improvement in stability for the hydrogenation activity with an increase of H_2S co-

fed from 700 to 2100 ppm. The C-C cleavage deactivation constant decreases into a negative value with added H_2S because the C-C cleavage activity increases with time. This results in an increase in CO_x and other C_1/C_2 products with time on stream. While added H_2S helped the stability of the deoxygenation and hydrogenation activity for the $NiMoS_x$ catalyst, there was still deactivation observed. However, the deoxygenation and hydrogenation rate constants decreased by 10 and 5 times respectively when H_2S was co-fed with glycerol. The H_2S thus plays three roles in the reaction: 1) it improves the deoxygenation and hydrogenation activity, 2) it reduces initial C-C cleavage and 3) it improves the catalyst stability.

Table 2.2: Glycerol HDO over NiMoOx and NiMoSx catalyst with varying H2S co-feed, showing conversions and deactivation constants. Reaction conditions: 400°C, 270 psig, 360 contact time.

Catalyst	**$NiMoO_x$**	**$NiMoS_x$**	**$NiMoS_x$**	**$NiMoS_x$**
H_2S (ppm)	0	0	700	2100
Conversion (%)	100	100	100	100
ToS (h)	3.0	3.3	2.9	3.0
Carbon Balance (%)	102.3	101.2	100.4	98.0
Deoxygenation (%)	82.5	70.2	77.4	82.7
$\beta_{1,deox}$ (h^{-1})*10^2	2.22	2.12	0.13	0.17
Hydrogenation (%)	62.9	42.3	58.8	72.5
$\beta_{1,hydrog}$ (h^{-1})*10^2	4.34	4.50	1.26	0.76
C-C Cleavage (%)	11.8	28.0	30.6	23.0
$\beta_{1,cc}$ (h^{-1})*10^2	0.59	1.21	-0.79	-1.07
C3:C2:C1	1:0.17:0.12	1:0.33:0.42	1:0.45:0.49	1:0.35:0.31
Carbon Yield (%)				
Alkanes/alkenes	72.4	59.5	74.3	80.2
Oxygenates	17.5	18.4	5.4	4.5
CO_x	5.3	18.9	18.0	12.1
Unidentified	7.0	4.4	2.0	1.2

2.2.2. Glycerol HDO at varying contact times

Figure 2.6 shows the product yields for glycerol HDO without H_2S co-feed over the $NiMoS_x$ catalyst with varying contact time. The deoxygenation and hydrogenation of glycerol increases with contact time. The alkane/alkene yield increases with contact time, from 1.9% at 3 s to 59.5% at 360 s. The oxygenate yield initially increases with contact time, from 23.2% at 3 s to 43.5% at 45 s. The yield of oxygenated products then decreases to 18.4% at 360 s due to an increase in intermediate oxygenates converted to alkanes/alkenes. The C-C cleavage increases with contact time from 3.3% at 3 s to 28.0% at 360 s with a resulting increase in CO_x yield. At a contact time of 360 s, the carbon balance was >98.0% with a fresh catalyst for all experiments. The products from glycerol HDO at contact times of 3 and 45 s were dark brown. At these same contact times the reactor plugged after 8 hours TOS. Because of this, stability studies were not run at short contact times. At a 3 s contact time, the carbon balance was 80.0%. The missing products are likely oxygenates oligomers that are not detected using the analytical techniques in this study. These results highlight that the oxygenated intermediates produced from glycerol (a thermally stable molecule) are thermally unstable and can form oligomers during the reaction. This also complicates the identification of primary products.

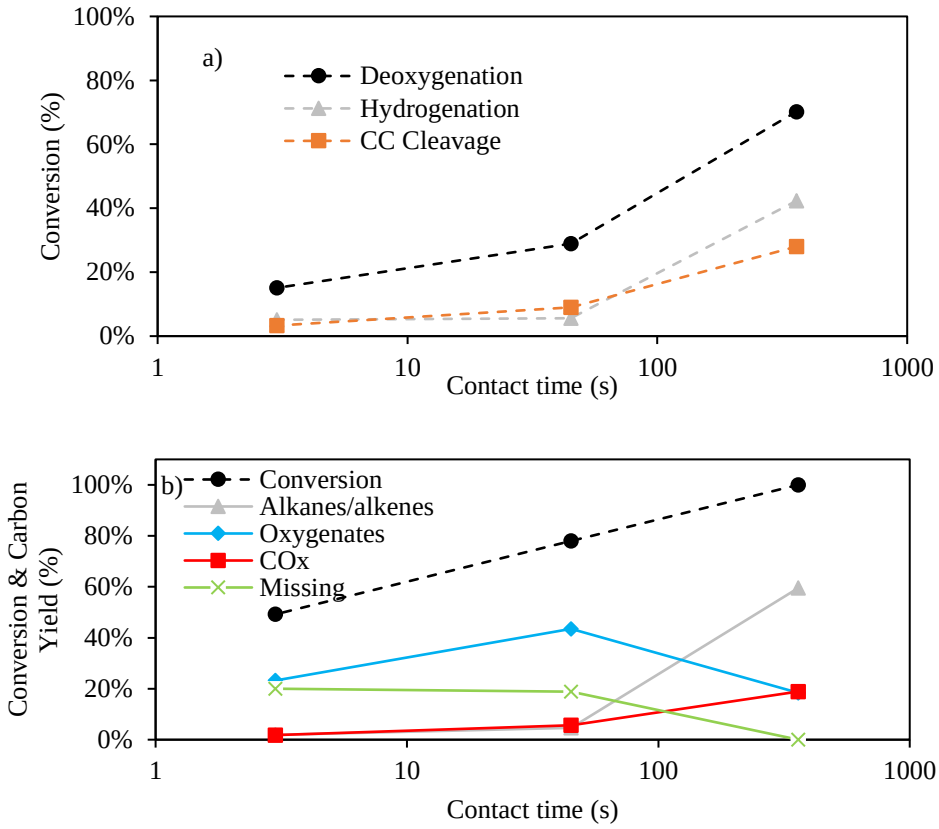

Figure 2.6: Glycerol HDO over NiMoSx catalyst with no H2S co-feed, showing conversion and product yield with varying contact times. Reaction conditions: 400°C, 270 psig, contact times of 3-360 s.

Table 2.3 shows the product selectivities from glycerol HDO over $NiMoS_x$ at contact times varying from 3 to 360 s with no sulfur co-feed and at a contact time of 3 s with a 2100 ppm H_2S co-feed. The carbon balance for the 3 s contact time with the 2100 ppm H_2S was higher than the carbon balance without the H_2S co-feed at a low conversion of 5.5%. The selectivities are normalized to sum to 100% to avoid convolution from the >100% carbon balances. Without a sulfur co-feed the selectivities of converted glycerol at a contact time of 3 s are 24.6% allyl alcohol, 8.8% hydroxyacetone, 7.3% acrolein, and a missing carbon selectivity of 34.8% at 49.2% conversion. With an increase in contact time to 45 s, the major product selectivities are

13.1% propionaldehyde, 11.9% hydroxyacetone, 11.1% acrolein, 8.9% allyl alcohol, 7.1% acetaldehyde, and a missing carbon selectivity of 17.4% at 76.0% conversion. From 3 to 45 s, the hydrogenation barely increases with the major products for both being mostly unsaturated. At a contact time of 360 s, the major products are mostly alkanes/alkenes, CO_x, and saturated oxygenates with no missing carbon at 100% conversion. The "others" group consisted of condensation products such as ethers and acetals like 5-hydroxy-1,3-dioxane. At a contact time of 3 s with an H_2S co-feed of 2100 ppm the selectivities were 41.4% allyl alcohol, 20.9% hydroxyacetone, 9.4% acrolein, 8.7% methanol, 7.7% propylene, 3.8% acetaldehyde, and no missing carbon at 5.5% conversion. At a short contact time, adding H_2S to the co-feed appeared to lower the catalyst activity to deoxygenation, hydrogenation, and C-C cleavage while mitigating the loss of carbon through condensation reactions. This contrasts with the results at a contact time of 360s where the run at 2100 ppm H_2S shows higher activity than the run at 0 ppm H_2S. This could be due to inhibition by H_2S .[38,67]

Table 2.3: Glycerol HDO over NiMoSx catalyst, showing conversion and product yields with varying contact times. Reaction conditions: 400°C, 270 psig, contact times of 360 s.

Contact time (s)	**3**	**3**	**45**	**360**
H_2S (ppm)	**2100**	**0**	**0**	**0**
Conversion (%)	5.5	49.2	76.0	100.0
Carbon Balance (%)	102.4	82.9	86.7	101.2
Deoxygenation (%)	4.2	15.6	31.4	70.2
Hydrogenation (%)	1.8	5.7	6.1	42.3
C-C Cleavage (%)	0.6	3.3	9.8	28.0
C3:C2:C1	1:0.06:0.08	1:0.06:0.09	1:0.15:0.17	1:0.33:0.42
Carbon Selectivity (%)				
Alkanes/alkenes	**8.8**	**3.9**	**8.7**	**58.9**
Propane	0.2	0.0	0.1	16.5
Propylene	7.7	3.5	5.1	26.0
Ethane	0.0	0.1	0.4	11.0
Ethylene	0.2	0.1	0.8	1.9
Methane	0.6	0.2	0.3	3.5
Oxygenates	**91.1**	**48.9**	**57.6**	**18.2**
1-Propanol	0.0	0.0	0.1	4.4
Allyl alcohol	41.4	24.6	8.9	2.8
Propionaldehyde	2.4	1.5	13.1	1.6
Acrolein	9.4	7.3	11.1	0.1
Acetone	2.7	1.7	2.5	3.3
Hydroxyacetone	20.9	8.8	11.9	0.0
Ethanol	1.9	0.0	0.4	4.1
Acetaldehyde	3.8	2.9	7.1	0.9
Methanol	8.7	2.1	2.5	1.0
CO_x	0.0	**3.7**	**7.9**	**18.7**
CO	0.0	2.0	6.8	17.1
CO_2	0.0	1.7	1.1	1.6
Others	0.2	**4.4**	**5.7**	**2.2**
Missing	0.0	**34.8**	**17.4**	**0.0**

The proposed reaction pathway of glycerol HDO over a $NiMoS_x$ catalyst at hydropyrolysis conditions is shown in Figure 2.7. Glycerol first undergoes dehydration to produce hydroxyacetone or 3-hydroxypropionaldehyde. These products can then be hydrogenated to produce 1,2 propanediol and 1,3 propanediol. 1,2 propandiol can undergo dehydration reactions to produce acetone or allyl alcohol. Similarly 3-hydroxypropionaldehyde undergoes dehydration producing acrolein. Acrolein can then undergo hydrogenation to either propionaldehyde or allyl alcohol. Further hydrogenation and dehydration produces isopropanol, 1-propanol, propylene and propane. It is not clear when C-C cleavage occurs in this reaction pathway, however, hydroxyacetaldheyde, acetaldehyde, ethanol, ethylene, ethane, CO, CO_2, methanol, formaldehyde, and methane are all observed. At short contact times, the major observed C_2 product was acetaldehyde with low yields of hydroxyacetaldehyde observed in some samples. Either acetaldehyde or hydroxyacetaldehyde could be formed through multiple C-C cleavage pathways. At longer contact times, the C_2 products are mainly ethanol, ethylene, and ethane. The C_3 reaction pathway is less clear since the initial deoxygenation step occurs at either the primary or the secondary alcohol to form hydroxyacetone or 3-hydroxypropionaldehyde, respectively. Hydroxyacetone was observed as a major product at short contact times while 3-hydroxypropionaldehyde was only observed in small (<0.1% yield) quantities. 3-hydroxypropionaldehyde likely rapidly deoxygenates to form acrolein. Allyl alcohol was found to form selectively at a contact time of 3 s with and without a sulfur co-feed. Allyl alcohol could be formed through the hydrodeoxygenation of hydroxyacetone, the hydrodeoxygenation of hydroxypropionaldehyde, or the hydrogenation of acrolein. Some studies have shown selective production of allyl alcohol from glycerol claiming a hydrogen transfer mechanism where glycerol transfers hydrogen to acrolein to form allyl

alcohol selectively.[68-70] Future research is needed to measure the rates of these individual pathways but Figure 2-7 provides the general products that are produced from a glycerol hydrodeoxygenation.

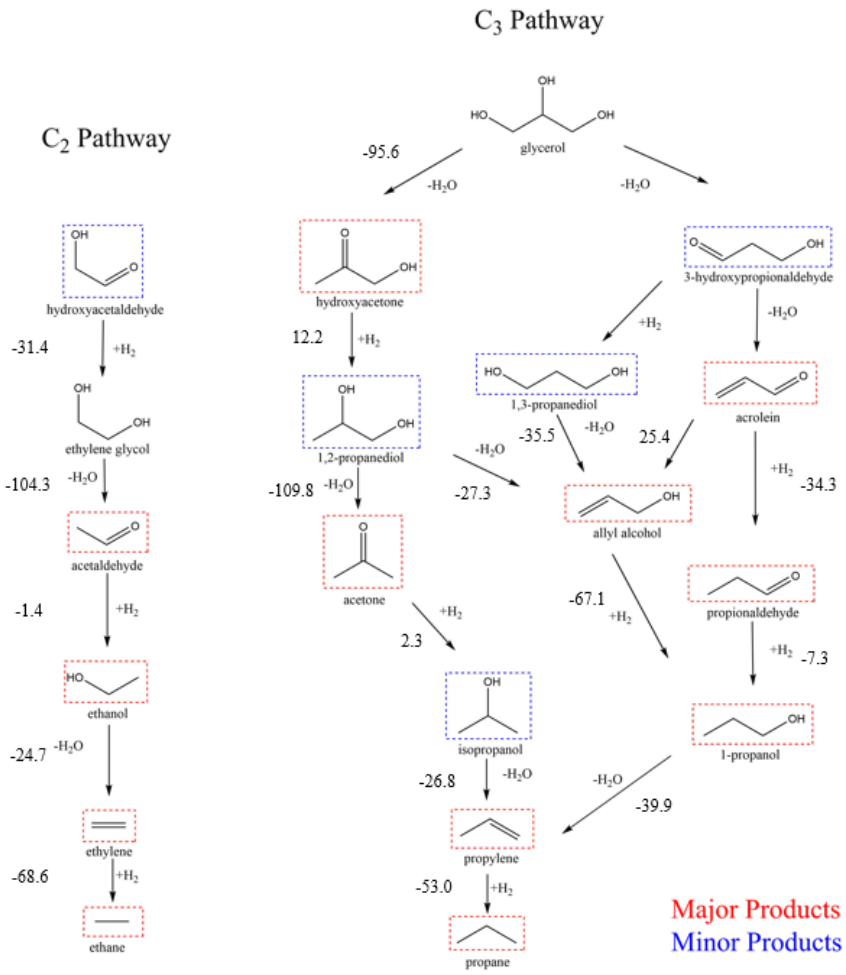

Figure 2.7: Proposed reaction network of glycerol HDO at hydropyrolysis conditions over a NiMoSx catalyst with the Gibbs free energies in kJ/mol calculated at 400°C.

DMSO can also be used as a sulfiding agent for laboratory studies for hydrotreating catalysts.[40,71] Table 2.3 shows the product comparison at 3 and 360 s contact times for glycerol HDO with a DMSO co-feed, an H_2S co-feed, and no H_2S co-feed. DMSO is commonly used

as a non-toxic sulfiding agent in hydrotreating reactions as it is converted to H_2S, water, and methane over a catalyst in a H_2 atmosphere.[71-72] The DMSO experiments contained enough DMSO to produce 2100 ppm H_2S if all DMSO was converted into methane, water, and H_2S. At 360 s the carbon balances of no co-feed, H_2S co-feed, and DMSO co-feed all show high carbon balances. Co-feeding DMSO as a sulfiding agent resulted in a 4 times higher deoxygenation deactivation constant and a 2 times higher hydrogenation deactivation constant compared with co-feeding H_2S gas at 2100 ppm. At a short contact time, DMSO as a co-feed resulted in a carbon balance of 59.2%. The major product was acrolein, with only a small amount of allyl alcohol compared to the other experiments at 3 s. This low carbon balance was due to DMSO thermally decomposing into methyl-mercaptan and formaldehyde and homogeneously reacting with glycerol and other intermediates. This hypothesis was confirmed through an experiment with no catalyst at the same conditions where the glycerol conversion was 52.3% with a carbon balance of 64.5%. These experiments show that H_2S is required to study $NiMoS_x$ catalysts at low conversion with oxygenated feeds.

Table 2.4: Glycerol HDO over NiMoSx catalyst with and without sulfur co-feeds, showing conversion and product yields with varying contact times. Reaction conditions: 400°C, 270 psig, 72.5-80 wt% glycerol and 0-7.5% DMSO in water

Co-feed	**DMSO**	**H_2S gas**	**None**	**DMSO**	**H_2S gas**	**None**
Contact time (s)	**3**	**3**	**3**	**360**	**360**	**360**
Conversion (%)	57.5	5.5	49.2	100.0	100.0	100.0
Carbon Balance (%)	59.2	102.4	82.9	106.2	98.0	101.2
Deoxygenation (%)	5.3	4.2	15.6	88.2	82.7	70.2
Hydrogenation (%)	2.9	1.8	5.7	73.6	72.5	42.3
C-C Cleavage (%)	0.8	0.6	3.3	25.4	23.0	28.0
$\beta_{1,deox}$ (h^{-1})*10^2	-	-	-	0.57	0.17	2.12
$\beta_{1,hydrog}$ (h^{-1})*10^2	-	-	-	1.28	0.76	4.50
$\beta_{1,cc}$ (h^{-1})*10^2	-	-	-	-0.36	-1.07	1.21
C3:C2:C1 Carbon Yield (%)	1:0.11:0.09	1:0.06:0.08	1:0.06:0.09	1:0.37:0.32	1:0.35:0.29	1:0.33:0.42
Alkanes/alkenes	**0.6**	**0.5**	**1.9**	**84.5**	**80.2**	**59.5**
Propane	0.0	0.0	0.0	38.4	51.0	16.7
Propylene	0.1	0.4	1.7	20.0	5.4	26.3
Ethane	0.1	0.0	0.0	19.1	18.2	11.1
Ethylene	0.1	0.0	0.1	0.5	0.1	1.9
Methane	0.4	0.0	0.1	6.5	5.5	3.5
Oxygenates	**7.8**	**6.8**	**23.2**	**6.4**	**4.5**	**18.4**
1-Propanol	0.4	0.0	0.0	2.6	1.3	4.4
Allyl alcohol	0.3	2.3	12.1	0.0	0.1	2.9
Propionaldehyde	0.2	0.1	0.0	0.1	0.0	1.6
Acrolein	5.1	1.7	3.6	0.0	0.0	0.1
Acetone	0.2	0.7	0.8	0.3	0.6	3.3
Hydroxyacetone	0.8	1.4	4.3	0.0	0.0	0.0
Ethanol	0.0	0.1	0.0	3.4	2.0	4.2
Acetaldehyde	0.7	0.3	1.4	0.0	0.2	0.8
Methanol	0.1	0.5	1.0	0.0	0.3	1.0
CO_x	**0.1**	0.0	**1.8**	**13.1**	**12.1**	**18.9**
CO	0.1	0.0	0.9	12.2	11.5	17.3
CO_2	0.0	0.0	0.8	0.9	0.6	1.6
Unidentified	**8.2**	**0.6**	**2.2**	**2.2**	**1.2**	**2.2**
Missing	**40.8**	**0.0**	**19.9**	**0.0**	**2.0**	**0.0**

2.2.3. Catalyst characterization

The BET surface areas and carbon content of fresh and spent catalysts after 30 h of glycerol HDO are shown in Table 2.5. The carbon content was calculated based on temperature programmed oxidation (TPO) and quantification of the resulting CO_2 and CO over time. The BET surface area of the fresh $NiMoS_x$ after sulfiding and passivation was 143.7 m^2/g. The spent catalyst after glycerol HDO with no H_2S co-feed had a BET surface area of 60.4 m^2/g with a carbon content of 23.45%. The spent catalyst from the glycerol HDO experiment with 2100 ppm had a BET surface area of 81.2 m^2/g with a carbon content of 1.93%. The carbon content difference indicates the deactivation could be largely caused by coking since the deactivation of $NiMoS_x$ was much higher with no H_2S co-feed than with 2100 ppm H_2S. The coking could be occurring due to a phase change on the catalyst surface caused by removal of sulfur from the MoS_x basal plane.[35,37] The reduction in surface area is not proportional to the carbon content.

Figure 2.8 shows the results from TPO of the spent catalyst after 30 h TOS of glycerol HDO with 0 ppm H_2S co-fed. The carbon was removed by 350°C while the sulfur was not removed until 500°C, indicating catalyst regeneration would require a calcination step of at least 500°C before re-sulfiding. The spent catalyst after 30 h TOS of glycerol HDO with 2100 ppm H_2S co-feed showed 11% more SO_2 per gram catalyst during TPO than the catalyst from the 0 ppm H_2S run at the same reaction and TPO conditions. This was calculated with the assumption that the coke on the catalyst was 85 wt% carbon. This indicates that the deactivation of the catalyst also causes a small loss of sulfur from the catalyst. This minor loss

of sulfur indicates the sulfur is not removed from the bulk catalyst, but likely the surface of the catalyst. After multiple glycerol HDO reactions followed by regeneration through calcination and sulfiding, the surface area of the $NiMoS_x/Al_2O_3$ was 128.1 m^2/g. This could be due to sintering of the active $NiMoS_x$ planar structure resulting in a loss of surface area and active Ni-Mo-S edge sites.[37,73-74]

Table 2.4: Characterization of NiMoSx catalyst before and after Glycerol HDO run for 30 h at a contact time of 360 s.

Catalyst	BET Surface Area (m^2/g)	Carbon (wt%)
Fresh $NiMoS_x$	143.7	-
Spent $NiMoS_x$ (2100 ppm H_2S)	81.2	1.93%
Spent $NiMoS_x$ (0 ppm H_2S)	60.4	23.45%
Regenerated $NiMoS_x$	128.1	-

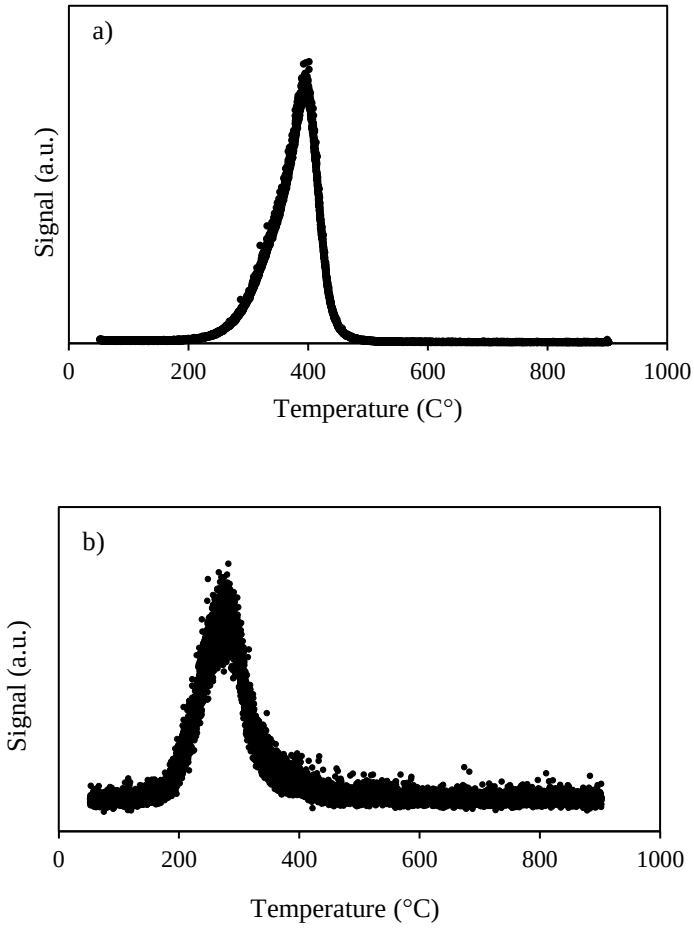

Figure 2.8: MS signal for a) 44 m/z (CO2) and b) 64 m/z (SO2) during the temperature programmed oxidation (TPO) of spent NiMoSx catalyst after 30 h of glycerol HDO with 0 ppm H2S co-feed at a contact time of 360 s. Conditions: 50 mL/min of 10% O2 in He

2.3. Conclusions

Standard NiMo hydrotreating catalysts can catalyze several classes of reactions for conversion of oxygenated biomass feedstocks including dehydration, C-C cleavage, deoxygenation, and hydrogenation. The major products of glycerol hydrodeoxygenation at short contact times were found to be unsaturated oxygenates such as allyl alcohol, acrolein, hydroxyacetone, and acetaldehyde. The major products at longer contact times were alkanes/alkenes, CO_x, and saturated alcohols such as propylene, propane, ethylene, methane, CO, methanol, ethanol, and propanol. The initial rate of deoxygenation and hydrogenation for glycerol were found to be lower for a $NiMoS_x$ catalyst compared to the $NiMoO_x$ catalyst. The initial rate of C-C cleavage conversions was higher for the $NiMoS_x$ catalyst compared to the $NiMoO_x$ catalyst. The $NiMoS_x$ and $NiMoO_x$ catalyst both deactivate at similar deactivation rates when no sulfur is added in the feed. The deactivation rate constants decrease according to the following order: hydrogenation > deoxygenation > C-C cleavage. The catalyst stability improves when sulfur is added to the feed as either H_2S or DMSO. DMSO decomposes and reacts homogeneously with glycerol to form condensation products at short contact times resulting in a low carbon balance. Co-feeding H_2S during hydrodeoxygenation improved the stability of the deoxygenation and hydrogenation activities up 12 and 6 times respectively, while the C-C cleavage deactivation rate constant becomes negative, resulting in an increase in C-C cleavage activity over time with an H2S co-feed. A major cause of deactivation is carbon deposition on spent catalysts. The carbon content of spent $NiMoS_x$ catalysts after 30 h of glycerol HDO with 0 and 2100 ppm H_2S in the feed were 23.45 and 1.93 wt% respectively, resulting in BET surface area reductions of 43.5% and 58.4% of the fresh $NiMoS_x$ catalyst

surface. At a shorter contact time, the activity of the $NiMoS_x$ catalyst was lower when 2100 ppm H_2S was co-fed compared to no sulfur co-feed but resulted in a significantly improved carbon balance.

3. Hydropyrolysis of Biomass with a Sand-bath heated semi-batch reactor

3.1. Scope

In the previous chapter, glycerol was utilized as a model compound and hydrodeoxygenated at hydropyrolysis conditions. The result of these experiments elucidated important stability and reaction chemistry information for hydrodeoxygenation of polyoxygenated aliphatic compounds. To effectively study the reaction chemistry of biomass hydropyrolysis, an analytical microreactor was designed for operation at hydropyrolysis conditions. This chapter will explore the product composition of maple wood, cellulose, and lignin hydropyrolysis.

3.2. Experimental

3.2.1. Catalyst Preparation

A γ-alumina supported NiMo catalyst from Albemarle Catalyst Company was received as an oxide. The catalyst was pretreated in batches by flowing 4 wt% dimethyl disulfide (DMDS) in heptane with an Eldex Optos Model 1 piston pump at a WHSV of 2 h^{-1} and H_2 gas at a GHSV of 600 h^{-1} while carefully ramping the temperature as shown in Figure 3.1. Afterwards, the catalyst was cooled under argon flow to room temperature where the sulfided catalyst was passivated with air before removing from the reactor. Before each batch experiment, the catalyst and biomass were mixed and placed in a ¼” stainless steel reactor between quartz wool plugs.

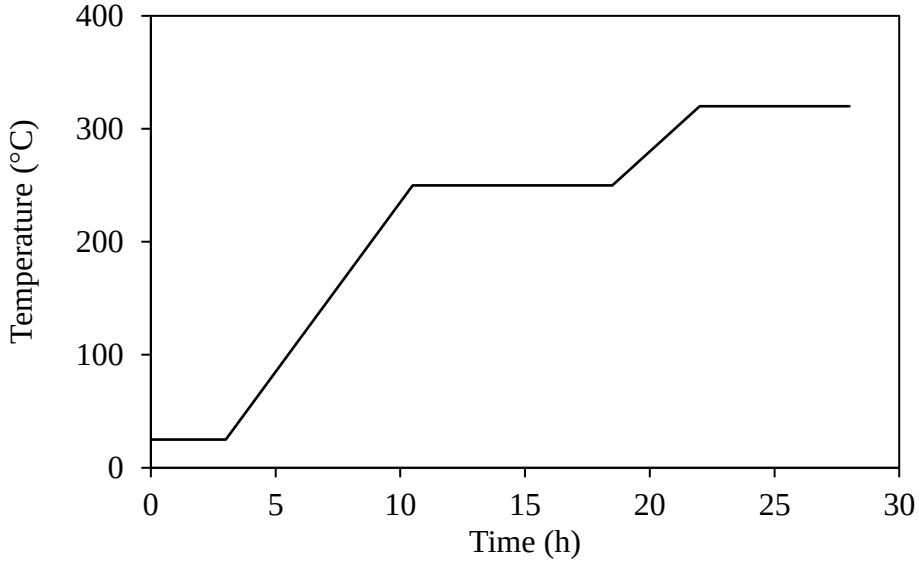

Figure 3.1: Reactor temperature over time during the sulfiding pre-treatment of the NiMoOx catalyst.

3.2.2. Catalyst Characterization

The spent catalysts were characterized via temperature-programmed oxidation (TPO) using a Micrometrics AutoChem II 2920 instrument equipped with a Cirrus 2 Quadrupole Mass Spectrometer. During TPO, 50 mg of catalyst was loaded into a quartz u-tube and dried for 2 h at 150°C with 50 mL min^{-1} He flow. After cooling to room temperature, the sample was heated at a rate of 10°C min^{-1} to 700°C with 50 mL min^{-1} of 10% O_2 in He. The CO_2, CO, and SO_2 were detected using mass spectrometry. The CO_2 and CO were calibrated to quantify the carbon from oxidation through integration. The surface area before and after reaction was determined by the Brunauer-Emmett-Teller (BET) method using a Micrometrics ASAP 2020 Plus instrument.

3.2.3. Experimental Setup

Figure 3.2 shows a schematic of the sand-bath heated hydropyrolysis system designed for high-throughput experiments of fast pyrolysis and in-situ hydrodeoxygenation of solid biomass. Reactors were made of ¼" diameter and 0.014" wall thickness 316L stainless steel tubes loaded with mixed biomass and catalyst. $NiMoS_x$ catalyst was loaded pre-sulfided and passivated. Thin-walled tubing was utilized for ease of loading and fast heating rates. The reactor system was supplied ultrahigh purity (UHP) grade H_2 (Airgas), 2% H_2S in H_2 (Airgas), and UHP Argon (airgas) via mass flow controllers (Brooks). Before reaction, the reactor was pressurized and leak tested with UHP Argon and then with hydrogen. To prepare for reaction, the sand-bath was heated, the line between the reactor and the condenser was heated to 300°C, and the condenser was filled with methanol (MeOH) and cooled to 0°C in an ice water bath. At the start of reaction, the hydrogen flow rate was set to 300 mL/min and the sand-bath was raised so the reactor was submerged in the fluidized sand. Immediately after a timer was started and the gas line was switched to a 150 mL stainless steel vessel. The gas is then collected for 3 min, at which point the timer was stopped and the gas was switched to vent. Gas products were generated mostly within the first minute of reaction, and the reaction was mostly complete after two minutes. The sand-bath was then lowered, and the gas flow was shut off. The pressure of the pressurized vessel was recorded before sampling the gas by opening a needle valve to allow flow to the online gas GC. The condenser was sampled and depressurized before pumping 3 mL of MeOH through the dip tube and sampled to ensure all product was collected. The pumping of methanol through the dip tube after reaction was found to be necessary to collect heavy compounds that may have deposited on the cold wall of the dip tube.

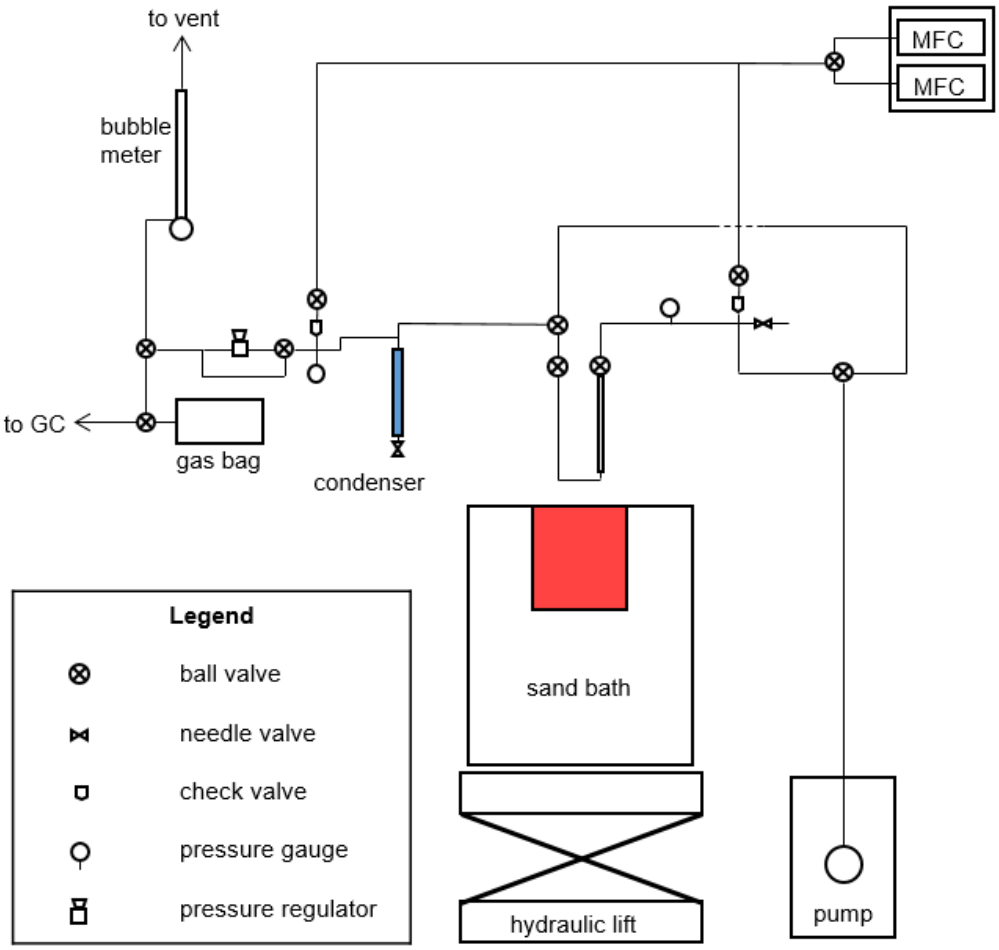

Figure 3.2: A simplified schematic of the semi-batch hydropyrolysis reactor.

3.2.4. Product Analysis

After an experiment, the gas sampling vessel is slowly evacuated through a needle valve and sent to a gas GC. Gas samples were analyzed by an online Shimadzu GC-2014 instrument equipped with a sample loop and both a thermal conductivity detector (TCD) and flame ionization detector (FID). The TCD detector was used to quantify CO and CO_2 while the FID detector was used to quantify C1-C4 hydrocarbons. Permanent gases were identified and calibrated with triplicate single point calibration using SCOTTY specialty gas mixtures, resulting in < 2% relative standard error. Liquid samples were identified using a Shimadzu GC-2010 instrument with an RTX-VMS column equipped with a Shimadzu GCMS-QP2010 mass spectrometer and quantified using a Shimadzu GC-2010 instrument equipped with an FID and RTX-VMS column. The methods for each GC were similar, to allow for similar elution times across the GC-FID and GC-MS injections. Over 20 major liquid products were calibrated using 4-point calibrations. The sensitivities of other products were calculated using their effective carbon numbers (ECN) and a reference compound with similar functionality.[65] Unassigned GC observable compounds were classified by carbon count, oxygen count, and molecular weight and their response factors were normalized by carbon number. This resulted in grouping of compounds such as “C9 aromatic monomer” for substituted benzene compounds or “C12 polyaromatic” for substituted naphthalenes or indanes.

High boiling species were quantified utilizing GC-FID with Restek MXT-1HT Sim Dist non-polar column with the following program: 5 min hold at 40°, ramp to 415°C at 15°C/min, 5 min hold. Any compound eluting after dodecane was considered “high-boiling”, and the peak areas of these compounds were summed and quantified assuming an ECN equal

to 4-propyl-guaiacol. Dimer and trimer peaks eluted as large, wide peaks composed of many individual peaks, requiring baseline subtraction using solvent blank injections. The total carbon balance was calculated based on all analyzed products divided by the carbon present in the cellulose, lignin, or maple wood. Maple wood, cellulose (Avicel PH-101), and maple wood lignin were used as a feedstock during these experiments. Lignin feedstock was extracted from maple wood through the GVL extraction process shown by Luterbacher et al..[75] The hemicellulose, cellulose, lignin, and ash content were measured utilizing the procedure shown by the National Renewable Energy Laboratory (NREL).[76] Maple wood feed was first ground and sieved between 45-80 mesh size before reaction. Each biomass feed was measured for moisture content before use and contained between 5-8% moisture.

3.2.5. Fourier Transform Ion Cyclotron Resonance Spectroscopy (FT-ICRMS)

Liquid samples from hydropyrolysis experiments were analyzed via fourier transform ion cyclotron resonance spectroscopy (FT-ICRMS). Spectrometric data were acquired using a Bruker solariX XR FT-ICRMS with a 15 T shielded superconducting magnet. Experiment parameters, acquisition, and processing were performed on Bruker Compass DataAnalysis 4.5 and Bruker Daltonics ftmsControl 2.1.0 software. Both atmospheric pressure chemical ionization (APCI) and atmospheric pressure photoionization (APPI) were used to analyze each sample. Injected samples had a product concentration of 50-200 ppm in methanol and were injected using a syringe pump using flow rates of 100-300 µL/h. The data were processed using a sine-squared apodization method in absorption mode. Elemental formulas for relevant peaks were assigned using PetroOrg software.[77]

3.3. Results and Discussion

3.3.1. Hydropyrolysis of Cellulose, Lignin, and Maple Wood

The hydropyrolysis of various biomass types was performed using the semi-batch hydropyrolysis reactor. During a cellulose hydropyrolysis experiment, a 1/16" thermocouple was placed in the middle (radially and axially) of the catalyst/biomass bed. The temperature of the bed was tracked over time and sampled every 10 ms utilizing DataQ DI-2008 data logger system with WinDaq software. Figure 3.3 shows the measured heating rate plotted against bed temperature. The heating rate peaks at 20°C/s at 120°C before falling to 5°C/s at 140°C. The dip in heating rate starting around 140°C may be due to water vaporizing. The heating rate then increases to 16°C/s at 220°C before steadily lowering. Lignocellulosic biomass pyrolyzes mostly in the range of 200-400°C.[10] A time-average heating rate of 9.7 °C/s was measured in this range.

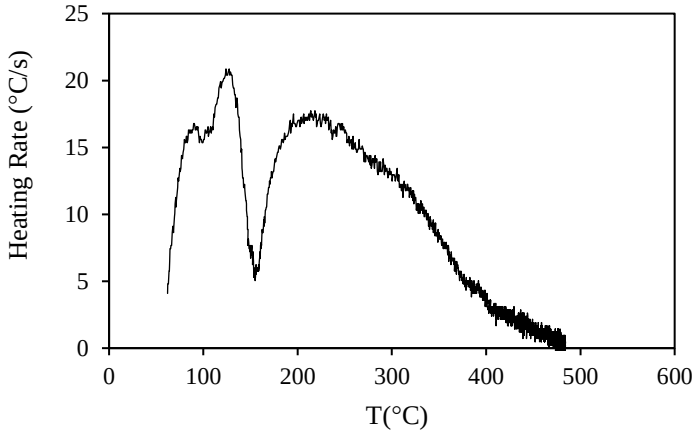

Figure 3.3: Temperature vs heating rate (TC in middle of catalyst bed). Reaction conditions: 500°C sandbath, 270 psi, 300 mL/min H2, 30 mg avicell cellulose, 300 mg passivated NiMoSx.

The hydropyrolysis of lignocellulosic biomass yields products from cellulose, hemicellulose, lignin, and secondary reactions between these intermediates.[78-79] Pyrolyzing cellulose and lignin separately can help elucidate this chemistry. The pyrolysis of hemicellulose was not investigated due to the similar reaction chemistry to cellulose hydropyrolysis. Table 3.1 shows yields from the hydropyrolysis of maple wood, lignin, and cellulose. The hydropyrolysis of lignin yielded 18.3% solids, 23.5% C_1-C_4 products, and 43.6% C_5+ products for a total of 86.3% overall yield. The C_1-C_4 products are mainly composed of methane, ethane, propane, ethylene, propylene, butylenes, ethanol, and acetaldehyde. The C_5+ products are mostly composed high boiling species (C_{13}+), C_8-C_{10} aromatic monomers, C_5-C_6 aliphatics, methyl-cyclohexanes, methyl, cyclopentanes, BTX, and poly-aromatics (C_{10}-C_{12}). A majority of C_5+ products from lignin are high boiling species of C_{13}+. These species range in boiling point from 220-420°C, composed of dimer and trimer lignin species. Dimer species may range from C_{12}-C_{22} but are mostly in the range of C_{15}-C_{18}. Trimer species may range from C_{18}-C_{33} but are mostly in the range of C_{21}-C_{27}. Lignin hydropyrolysis products are mostly deoxygenated, with only a 5.9% yield of oxygenates. The yield of other oxygenates was mostly composed of ethers, esters, and poly-oxygenates. Cellulose hydropyrolysis yielded 7.0% solids, 37.0% C_1-C_4 products, and 37.4% C_5+ products for a total of 88.9% overall yield. The C_1-C_4 products are mostly composed of CO_2, CO, methane, ethane, propane, ethylene, propylene, butylenes, butanes, acetaldehyde, propionaldehyde, butyraldehyde, and acetone. The C_5+ products are mainly composed of cyclopentanes, cyclopentenes, C_5-C_6 aliphatics, cyclohexanes, BTX, cyclopentanones, and furans. No products with boiling points above 220°C were observed. Furans were mainly composed of furfural, 5-hydroxymethyl-furfural, and furan.

Cyclopentanones were mainly composed of cyclopentanone and methyl cyclopentanone. Cyclopentanes and cyclopentanone are likely formed through furfuryl alcohol rearrangement.[80-81] Methyl cyclopentanones and methyl cyclopentanes are likely formed by rearrangement of 5-hydroxymethyl furfural. The hydropyrolysis of maple wood yielded 13.9% solids, 39.6% C_1-C_4 products, and 29.2% C_5+ products for a total product yield of 88.8%. The C_1-C_4 products were mainly methane, ethylene, CO, CO_2, acetic acid, and propylene. Only 0.3% yield of acetic acid resulted from cellulose hydropyrolysis, while whole biomass hydropyrolysis yielded 2.1% likely due to the hemicellulose portion of whole biomass. C_5+ products were mostly composed of high boiling species, BTX, cyclopentanes, and aromatic monomers. While whole biomass hydropyrolysis products appears to be a combination of products from cellulose and lignin, biomass also appears to result in methane, propylene, and ethylene yields due to high C-C cleavage. Lignin and whole biomass hydropyrolysis products did not contain any observable methoxy aromatics and negligible phenolic yields (< 0.1% for all cases).

Table 3.1: Hydropyrolysis of 3 types of biomass over NiMoSx catalyst at a 10:1 catalyst:biomass ratio in a semi-batch reactor heated by a fluidized sandbath. Reaction conditions: 500°C sandbath, 270 psi, 300 mL/min H2, 30 mg biomass, 300 mg passive

Biomass	**Whole**	**Lignin**	**Cellulose**
		Yield (C%)	
Solids	13.9	18.3	7.0
Total	**88.8**	**86.3**	**88.9**
C_1-C_4	**39.6**	**23.5**	**37.0**
C_5+	**29.2**	**43.6**	**37.4**
CO_x	**2.7**	**1.9**	**5.3**
Hydrocarbons	**59.5**	**36.9**	**51.9**
Methane	15.4	8.6	4.7
C_2-C_3 aliphatics	16.8	4.6	9.1
C_4+ aliphatics	8.6	5.2	10.3
C_5-C_6 cyclopentanes	6.0	0.5	13.1
C_6-C_7 cyclohexanes	0.8	2.6	1.8
C_6-C_8 BTX	6.8	1.8	4.4
C_8-C_{10} aromatic monomer	3.2	13.1	0.2
C_{10}-C_{12} poly-aromatics	2.6	0.8	0.2
Oxygenates	**6.4**	**5.9**	**30.0**
C_2-C_4 aliphatic aldehydes	0.0	0.2	4.0
C_3-C_6 aliphatic ketones	1.1	1.2	4.4
C_5-C_6 cyclopentanones	0.0	0.0	2.2
C_2-C_3 aliphatic alcohols	0.6	0.5	1.6
C_4-C_6 furans	1.0	0.5	9.6
Acetic Acid	2.1	0.0	0.3
Other oxygenates	4.4	2.6	7.5
High boiling	4.5	21.2	0.0

Table 3.2 shows a fuel fraction approximation of the products of biomass hydropyrolysis at a catalyst:biomass ratio of 10:1. The fractions were split based on carbon number with the jet/diesel fraction including the "heavy" products detected on the high temperature GC. Lignin hydropyrolysis produced mainly jet/diesel ranged products (36.0 C%) with a substantial amount of light gases (10.6 C%), LPG (9.2 C%), and gasoline (8.6 C%). Cellulose hydropyrolysis produced mainly gasoline (38.5 C%) along with substantial yields of LPG (16.5 C%) and light gases (9.0 C%). The high jet/diesel yields from lignin and the high gasoline yields from cellulose are mostly expected, assuming limited C-C cleavage or C-C coupling compared to hydrodeoxygenation activity. Due to the substantial C-C cleavage activity of the $NiMoS_x$ catalyst, the lignin tails are cleaved to from C_1-C_3 products and the C_6 aliphatics from cellulose are cracked. Limited C-C coupling (trace product) is seen in all case with this catalyst. The hydropyrolysis of whole biomass produces mainly light gases (28.0 C%) with substantial yields of gasoline (23.8 C%), jet/diesel (10.6 C%), and LPG (9.0 C%). The yields of CO_x are highest from cellulose (5.3 C%), lowest from lignin (1.9 C%), and in-between from whole biomass (2.7 C%). Considering the yields from lignin and cellulose, the light gas yields from whole biomass are much higher at 28.0%. The high yields of light gases could be from hemicellulose, however, hemicellulose pyrolyzes at lower temperatures which would promote lower C-C cleavage activity. The total gasoline + jet/diesel yields are 20.2 wt% which is lower than the 26 wt% from the IH2 process. However, the ratio of jet/diesel to gasoline yields was found to be 0.44 which is close to the 0.43 from the IH2 process. [27,64]

Table 3.2: C# yield during the hydropyrolysis of 3 types of biomass over NiMoSx catalyst at a 10:1 catalyst:biomass ratio in a semi-batch reactor heated by a fluidized sandbath. Reaction conditions: 500°C sandbath, 270 psi, 300 mL/min H2, 30 mg biomass

Biomass	**Whole**	**Lignin**	**Cellulose**
		Yield (C%)	
Light gases (C_1-C_2)	28.0	10.6	9.0
LPG (C_3-C_4)	9.0	9.2	16.5
Gasoline (C_5-C_8)	23.8	8.6	38.5
Jet/Diesel (C_9+)	10.6	36.0	4.1
CO_x	2.7	1.9	5.3
Unknown	4.4	2.6	7.5

3.3.2. Varying Catalyst:Biomass Ratios

The data for the hydropyrolysis of cellulose experiments are shown in Table 3.3. At a 5:1 catalyst:cellulose ratio a low overall yield of 66.2% is seen, with 7.1% solid yields, 18.3% C_1-C_4 yields, and 32.6% C_5+ yields. The 10:1 catalyst:cellulose products show higher overall yields at 88.9% with a solid content of 7.0%, C_1-C_4 content of 37.0%, and C_5+ content of 37.4%. The total yield increases at 20:1 catalyst:biomass ratio to 92.8%, with a C_1-C_4 yield of 38.7% and a C_5+ yield of 43.3%. Both the C_5+ and C_1-C_4 content increase due to higher overall yield and C-C cleavage. The hydrocarbon yields increase from 51.9% to 60.2% while the oxygenate yields decrease from 30.0% to 18.9%. No high boiling species are detected on the high temperature GC for cellulose experiments. The major oxygenate products are aldehydes, ketones, and furans which all decrease in yield with catalyst amount. The hydrocarbon products mostly increase, with the methane increasing from 1.5% at 5:1, to 4.7% at 10:1, to 17.6% at

20:1 catalyst:biomass ratio. Overall yields appear to increase with catalyst amount, but also result in more C-C cleavage.

The co-feeding of H_2S with H_2 improved the stability of $NiMoS_x$ catalysts during glycerol HDO by over 10 times for deoxygenation, but also lowered the activity of the catalyst, as shown in Table 2.2. For cellulose hydropyrolysis, the overall gas/liquid yields decreased from 88.9% to 53.9% when introducing 2100 ppm H_2S. Both hydrocarbons and oxygenated products decreased, with the only notable product yield difference being aldehyde yields of 0% and 2.6% alcohol yields compared to 4.0% aldehyde yields and 1.6% alcohol yields with 0 ppm H_2S. This indicates the H_2S may help the hydrogenation of aldehydes to alcohols. This is similar to what was seen with glycerol HDO where 2100 ppm H_2S yielded little aldehydes with the major products having primary alcohol functionality. The methane yield increases from 4.6% to 8.2% for the 2100 ppm H_2S. The 2100 ppm H_2S appears to lower the activity of the catalyst, resulting in lower overall yields of products. This is likely due to unstable products not being observable in the GC, like the 5:1 catalyst:biomass ratio experiment. The H_2S may result in sulfonated intermediates not detected by the GC.

Table 3.3: Hydropyrolysis of avicell cellulose over NiMoSx catalyst in a semi-batch reactor heated by a fluidized sandbath. Reaction conditions: 500°C sandbath, 270 psi, 300 mL/min H2, 30-100 mg avicell cellulose, 100-300 mg passivated NiMoSx.

Cat:Bio Ratio	**5:1**	**10:1**	**20:1**	**10:1**
H_2S (ppm)	**0**	**0**	**0**	**2100**
		Yield (C%)		
Solids	7.1	7.0	6.5	7.0
Total	66.2	**88.9**	92.8	**53.9**
C_1-C_4	18.3	**37.0**	38.7	**20.1**
C_5+	32.6	**37.4**	43.3	**21.6**
CO_x	3.7	**5.3**	7.2	**2.1**
Hydrocarbons	21.8	**51.9**	60.2	**28.2**
Methane	1.5	4.7	17.6	8.2
C_2-C_3 aliphatics	3.7	9.1	11.7	6.3
C_4+ aliphatics	4.8	10.3	10.8	4.4
C_5-C_6 cyclopentanes	7.4	13.1	13.8	5.0
C_6-C_7 cyclohexanes	1.0	1.8	1.7	0.2
C_6-C_8 BTX	2.2	4.4	4.3	2.5
C_8-C_{10} aromatic monomer	1.2	0.2	0.2	0.1
C_{10}-C_{12} poly-aromatics	1.0	0.2	0.1	1.3
Oxygenates	33.6	**30.0**	18.9	**15.8**
C_2-C_4 aliphatic aldehydes	6.7	4.0	1.2	0.0
C_3-C_6 aliphatic ketones	4.7	4.4	3.2	1.2
C_5-C_6 cyclopentanones	2.4	2.2	0.8	2.7
C_2-C_3 aliphatic alcohols	1.3	1.6	0.3	2.6
C_4-C_6 furans	9.8	9.6	8.0	5.2
Acetic Acid	0.4	0.3	0.0	0.3
Other oxygenate	8.2	7.5	5.4	4.3

Product yields from maple wood hydropyrolysis at varying catalyst:biomass ratios are shown in Table 3.4. At 10:1 catalyst:biomass ratio, the total product yields are 88.8 C%, with 59.5 C% yield of hydrocarbons, 6.4% yield of oxygenates, and 4.5% yield of high boiling. With a decrease in catalyst:biomass ratio from 10:1 to 5:1, the overall product yields decrease from 88.8 to 81.2 C%. The oxygenate yields increase from 6.4 C% to 23.5 C% while the hydrocarbon yields decrease from, 59.5 C% to 31.9 C% due to lower deoxygenation. With an increase in catalyst:biomass ratio from 10:1 to 20:1, the overall liquid and gas product yields increase from 58.9 to 85.2 C%, with C_1-C_4 increasing from 39.6 to 52.9 C% and C_5+ products decreasing from 29.2 to 23.3 C%. While the yields are higher overall, the heavy product yields are substantially lower due to high C-C cleavage activity. Table 3.5 shows the yield of products sorted by C# for the same wood hydropyrolysis experiments.

Table 3.4: Hydropyrolysis of maple wood over NiMoSx catalyst at varying catalyst:biomass ratios in a semi-batch reactor heated by a fluidized sandbath. Reaction conditions: 500°C sandbath, 270 psi, 300 mL/min H2, 30 mg biomass, 300 mg passivated NiMoSx.

Cat:Bio	**5:1**	**10:1**	**20:1**
		Yield (C%)	
Solids	14.2	13.9	N/A
Total	**81.2**	**88.8**	**85.2**
C_1-C_4	**36.4**	**39.6**	**52.9**
C_5+	**26.1**	**29.2**	**23.3**
CO_x	**2.2**	**2.7**	**4.0**
Hydrocarbons	**31.9**	**59.5**	**67.0**
Methane	8.9	15.4	29.3
C_2-C_3 aliphatics	8.7	16.8	17.8
C_4+ aliphatics	4.3	8.6	3.9
C_5-C_6 cyclopentanes	2.0	6.0	5.8
C_6-C_7 cyclohexanes	0.2	0.8	0.4
C_6-C_8 BTX	0.1	6.8	4.8
C_8-C_{10} aromatic monomer	4.7	3.2	3.9
C_{10}-C_{12} poly-aromatics	0.6	2.6	0.3
Oxygenates	**15.8**	**6.4**	**3.9**
C_2-C_4 aliphatic aldehydes	0.6	0.0	0.0
C_3-C_6 aliphatic ketones	6.0	1.1	2.6
C_5-C_6 cyclopentanones	0.0	0.0	0.0
C_2-C_3 aliphatic alcohols	1.4	0.6	0.4
C_4-C_6 furans	1.4	1.0	0.9
Acetic Acid	3.1	2.1	0.0
Other oxygenate	5.9	4.4	3.3
High boiling	9.6	4.5	2.3

Table 3.5: C# yield from the hydropyrolysis of maple wood over NiMoSx catalyst at varying catalyst:biomass ratios in a semi-batch reactor heated by a fluidized sandbath. Reaction conditions: 500°C sandbath, 270 psi, 300 mL/min H2, 30 mg biomass, 300 mg

C#	5:1	10:1	20:1
High Boil	9.6	4.5	2.3
7+	7.8	11.0	8.4
6	4.1	6.9	8.4
5	4.6	7.0	4.2
4	4.4	4.1	1.3
3	4.5	5.0	6.9
2	18.6	12.6	11.4
1	8.9	15.4	29.3
CO_x	2.2	2.7	4.0

Lignin hydropyrolysis was run using lignin separated via the γ-valerolactone **(**GVL) separation method developed by the Dumesic group.[12] This lignin is believed to be similar in chemical structure to the lignin found in whole biomass. Data from experiments with catalyst:biomass ratios varying from 5:1-20:1 are shown below in Table 3.6. At 10:1 catalyst:biomass ratio, the overall product yield was found to be 86.3 C%, with 43.6 C% yield to C_5+ products and 23.5% C_1-C_4 products. A 21.2% yield of high boiling products was approximated based on FID signal from products with boiling points >230°C.[13] These products are C_{12}+ and would include, naphthalenes, lignin dimers, lignin trimers, and heavy oligomeric species formed from C-C coupling. With a decrease in catalyst:biomass ratio to 5:1, the total product yields decrease from 86.3 C% to 50.7 C%, with substantially lower

aromatic monomer yields (13.1 to 1.3 C%) and high boiling yields (21.2 to 3.2 C%). Typically, experiments changing the catalyst:reactant ratio (WHSV in flow experiments) are performed to observe mechanisms via intermediates formed. With these experiments, this is not seen well due to poor carbon balance (< 50 C%). Because the intermediates formed during hydropyrolysis are incredibly reactive, lowering the catalyst amount results in higher oligomers formed which are not seen by GC. With increasing catalyst:biomass ratios from 10:1 to 20:1, the overall product yields increased from 86.3 to 98.5 C%, with C_1-C_4 and C_5+ product yields increasing from 23.5 to 35.0 C% and 43.6 to 45.2 C% respectively. Overall, there appears to be an increase in C-C cleavage with catalyst amount, with methane yields increasing from 8.6 to 26.3%, BTX yields increasing from 1.8 to 6.2 C%, and high boiling yields decreasing from 21.2 to 15.1 C%. While the catalyst appears to be necessary to stabilize the reactive pyrolysis intermediates, higher amounts of catalyst increase C-C cleavage activity. The solid yields were highest with a catalyst:biomass ratio of 5:1 at 20.9%, decreasing to 18.3% and 18.1% at 10:1 and 20:1 catalyst:biomass ratio, respectively. The solid content is mostly dependent on pyrolysis conditions rather than catalytic activity, so the similar solid yields are expected. The C_5+ content increases with catalyst:biomass ratio from 10.7% at 5:1,43.6% at 10:1, and 45.2% at 20:1.

Table 3.6: Hydropyrolysis of Lignin over NiMoSx catalyst at varying catalyst:biomass ratios in a semi-batch reactor heated by a fluidized sandbath. Reaction conditions: 500°C sandbath, 270 psi, 300 mL/min H2, 20-40 mg biomass, 200-400 mg passivated NiMo

	5:1	**10:1**	**20:1**
		Yield (C%)	
Solids	20.9	18.3	18.1
Total	**53.3**	**86.3**	**98.3**
C_1-C_4	**18.7**	**23.5**	**35.0**
C_5+	**10.7**	**43.6**	**45.2**
CO_x	**1.3**	**1.9**	**2.1**
Hydrocarbons	**21.5**	**36.9**	**57.2**
Methane	12.8	8.6	26.3
C_2-C_3 aliphatics	3.1	4.6	6.4
C_4+ aliphatics	0.2	5.2	1.2
C_5-C_6 cyclopentanes	0.6	0.5	1.0
C_6-C_7 cyclohexanes	0.2	2.6	1.2
C_6-C_8 BTX	1.6	1.8	6.2
C_8-C_{10} aromatic monomer	1.3	13.1	10.4
C_{10}-C_{12} poly-aromatics	1.8	0.8	4.5
Oxygenates	4.5	**5.9**	**3.4**
C_2-C_4 aliphatic aldehydes	0.1	0.2	0.0
C_3-C_6 aliphatic ketones	0.3	1.2	0.0
C_5-C_6 cyclopentanones	0.1	0.0	0.0
C_2-C_3 aliphatic alcohols	2.3	0.5	2.6
C_4-C_6 furans	0.2	0.5	0.1
Acetic Acids	0.0	0.0	0.0
C_6-C_8 phenolics	1.7	1.0	0.7
Other oxygenate	2.3	2.6	2.2
High boiling (220°C+)	3.2	21.2	15.1

3.3.3. Hydropyrolysis of maple wood at varying sand-bath temperatures

By changing the temperature of the fluidized sandbath, the heating rate and reaction temperature are varied. Table 3.7 shows the C% product yields from the hydropyrolysis of maple wood at varying temperatures. Maple wood hydropyrolysis at 500°C resulted in 13.9% solids, 37.5% C_1-C_4 products, and 30.2% C_5+ products for a total product yield of 86.7%. A decrease in sandbath temperature to 400°C resulted in 29.2% solids, 29.4% C_1-C_4., and 17.4% C_5+ products for a total yield of 82.4 C%. Maple wood hydropyrolysis at 600°C resulted in 10.8% solids, 42.6% C_1-C_4 products, and 29.5% C_5+ products for a total product yield of 83.7%. An increase in sandbath temperature results in lower solid yields and higher C_1-C_4 product yields. C_5+ product yields increased with temperature from 400-500°C and only slightly decreased in yield from 500-600°C. The high solid yields indicate hydropyrolysis at 400°C results in incomplete pyrolysis and slow heating rates.[58,82-83]

Table 3.7: Hydropyrolysis of maple wood over NiMoSx catalyst at variable temperatures in a semi-batch reactor heated by a fluidized sandbath. Reaction conditions: 400-600°C sandbath, 270 psi, 300 mL/min H2, 30 mg biomass, 300 mg passivated NiMoSx.

Temperature (°C)	**400**	**500**	**600**
		Yield (C%)	
Solids	29.2	13.9	10.8
Total	**82.4**	**86.7**	**83.7**
C_1-C_4	**29.4**	**37.5**	**42.6**
C_5+	**17.4**	**30.2**	**29.5**
CO_x	**2.2**	**2.7**	**3.8**
Hydrocarbons	**43.5**	**59.5**	**57.8**
Methane	11.7	15.4	17.0
C_2-C_3 aliphatics	15.9	16.8	16.3
C_4+ aliphatics	4.6	8.6	5.5
C_5-C_6 cyclopentanes	4.9	6.0	6.5
C_6-C_7 cyclohexanes	1.3	0.8	0.9
C_6-C_8 BTX	2.1	6.8	6.4
C_8-C_{10} aromatic monomer	2.7	3.2	3.7
C_{10}-C_{12} poly-aromatics	0.3	2.6	1.4
Oxygenates	**3.3**	**4.3**	**5.1**
C_2-C_4 aliphatic aldehydes	0.0	0.0	0.0
C_3-C_6 aliphatic ketones	0.3	1.1	1.7
C_5-C_6 cyclopentanones	0.0	0.0	0.7
C_2-C_3 aliphatic alcohols	1.8	0.6	1.0
C_4-C_6 furans	1.2	1.0	1.7
Other oxygenate	1.6	4.4	2.4
High boiling	2.6	4.5	3.8

3.3.4. FT-ICRMS of biomass hydropyrolysis heavy products

Liquid products from maple wood, maple wood lignin, and cellulose at varying catalyst:biomass ratios were studied using FT-ICR MS to approximate molecular formulas and molecular weights of heavier unassigned products (C12+). These data were plotted as carbon number against double-bond equivalents (DBE) to show the approximate chemical structure of the heavy products and their relative abundance. Figure 3.4 shows the FT-ICR MS plots of liquid products from maple wood hydropyrolysis at varying catalyst:biomass ratios corresponding to data in Table 3.4. Each product sample shows compound clusters ranging 14-20 C# and 5-14 DBE which would correspond with lignin dimer species. In each sample, peaks at (18C#, 12DBE) and (16C#, 10DBE) are observed, which may indicate aromatic lignin dimer species with unsaturated carbon tails. The peak observed at (18C#, 5DBE) may correspond to saturated lignin dimer species. The peak at (29C#, 5DBE) may correspond to saturated lignin trimer species for the 5:1 and 10:1 ratio samples. This peak was not seen for the 20:1 ratio sample, possibly due to further C-C cleavage with higher catalyst amount.

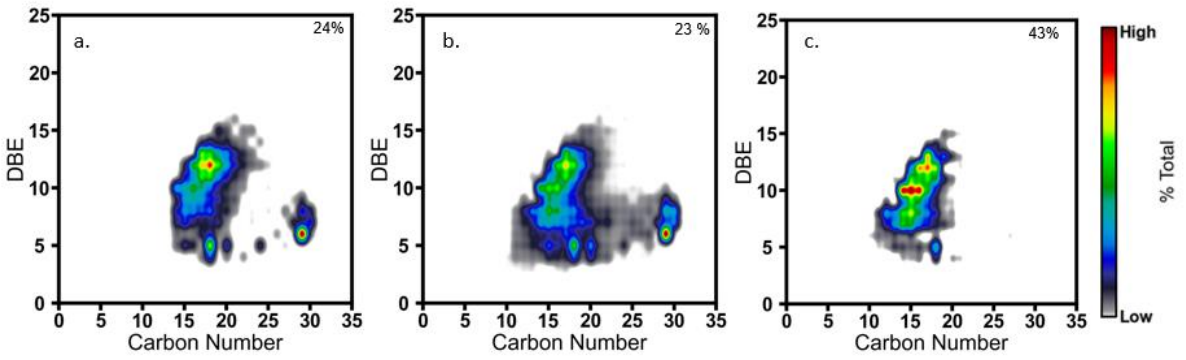

Figure 3.4: FT-ICR MS plots of liquid products from hydropyrolysis of maple wood at varying catalyst:biomass ratios. a) 5:1 b) 10:1 c) 20:1. Reaction conditions: 500°C sandbath, 270 psi, 300 mL/min H2, 20-40 mg biomass, 200-400 mg passivated NiMoSx.

Figure 3.5 shows FT-ICR MS plots for liquid samples from lignin hydropyrolysis at varying catalyst:biomass ratios corresponding to the data in Table 3.6. Each lignin product shows compound clusters ranging 14-20 C# and 5-14 DBE which would correspond with lignin dimer species, like what was seen for whole biomass in figure 4-4. The trimer peaks seen in Figure 3.4 for the 5:1 and 10:1 whole biomass experiments. The additional catalyst in the 20:1 experiment appeared to tighten the peak cluster, potentially due to the additional CC cleavage.

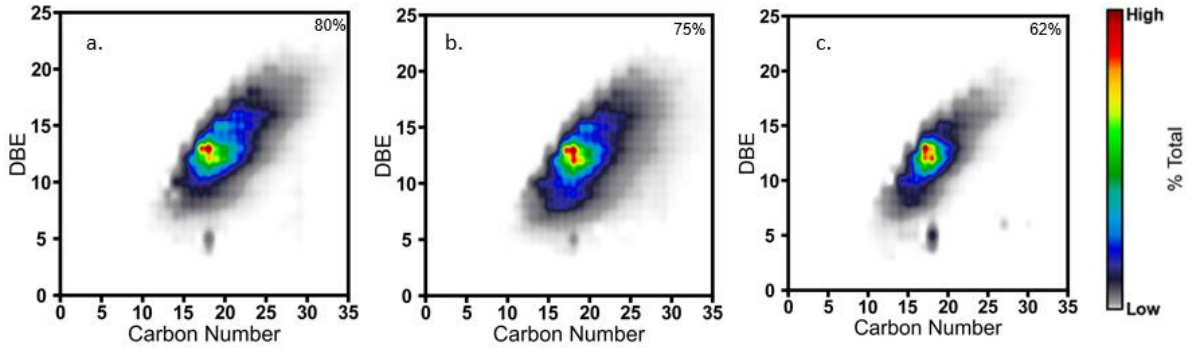

Figure 3.5: FT-ICR MS plots of liquid products from hydropyrolysis of lignin at varying catalyst:biomass ratios. a) 5:1 b) 10:1 c) 20:1. Reaction conditions: 500°C sandbath, 270 psi, 300 mL/min H2, 20-40 mg maple wood lignin, 200-400 mg passivated NiMoS

Figure 3.6 shows FT-ICR MS plots of liquid samples from hydropyrolysis of maple wood at varying temperatures (400-600°C). A peak at 18 C# and 5 DBE is present for all temperatures but is the most prominent peak for hydropyrolysis at 400°C, potentially corresponding to a partially hydrogenated lignin dimer species. Since lignin does not completely pyrolyze below 400°C, other products are not formed. Hydropyrolysis at 500°C and 600°C results in 14-20 C# and 5-14 DBE products indicating lignin dimer species. Trimer species at 28 C# and 6 DBE are seen at 500°C but not at 600°C, likely due to an increase in monomer cleavage.

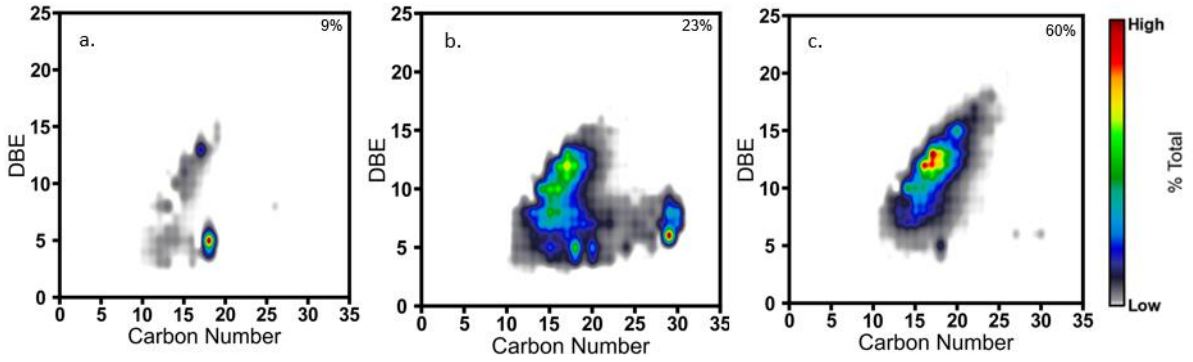

Figure 3.6: FT-ICR MS plots of liquid products from hydropyrolysis of maple wood at varying temperatures. a) 400°C b) 500°C c) 600°C. Reaction conditions: 400-600°C sandbath, 270 psi, 300 mL/min H2, 30 mg biomass, 300 mg passivated NiMoSx.

Figure 3.7 shows FT-ICR MS plots for liquid samples of maple wood hydropyrolysis at varying catalyst:biomass ratios, plotting carbon number against DBE and oxygen amount. At a catalyst:biomass ratio of 5:1 and 10:1 peaks at C18, DBE4 and C29, DBE6 are present with mostly 0-3 oxygen atoms. The broader peak ranging from C16, DBE8 to C22, DBE12 is only present for species with no oxygen for all catalyst:biomass ratios tested. This data shows that most heavy compounds collected and analyzed are largely deoxygenated. The unsaturated components ranging from DBE8-DBE12 are only present as non-oxygen containing species.

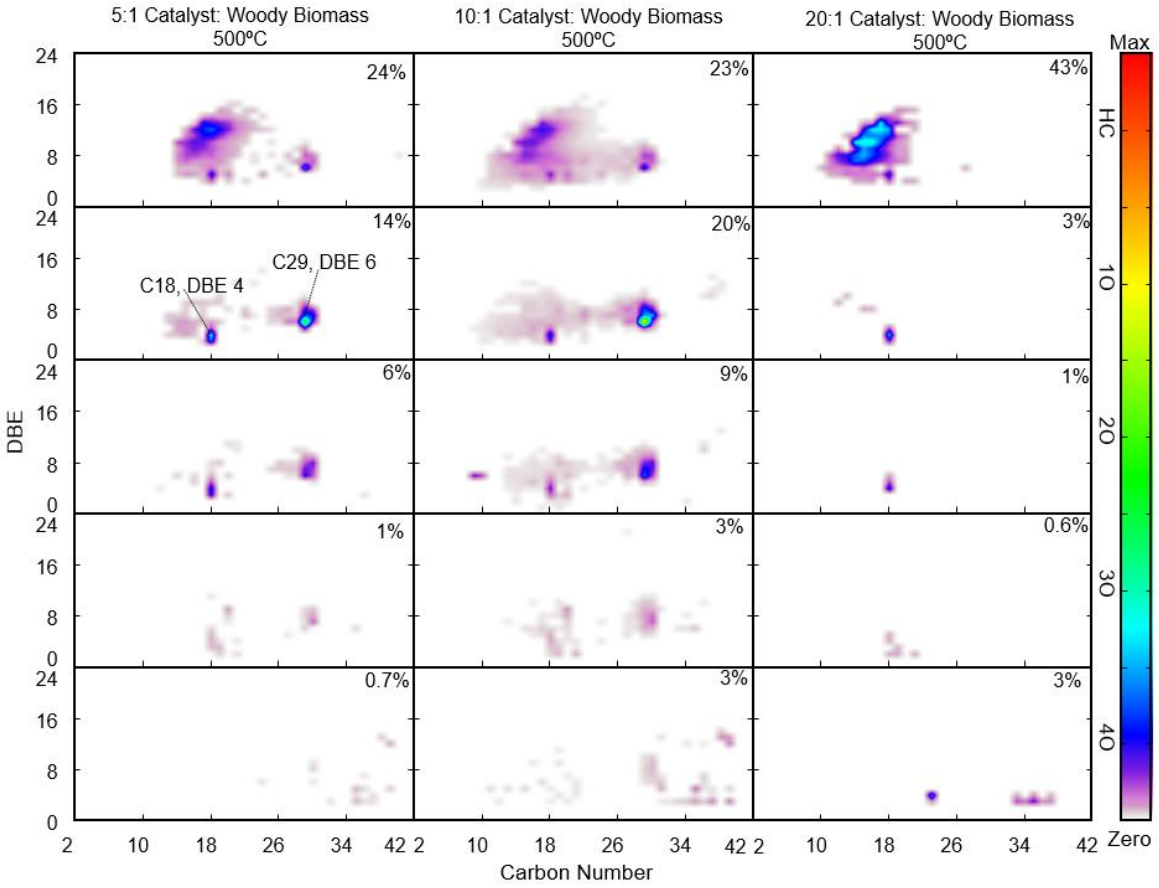

Figure 3.7: FT-ICR MS plots of liquid products from hydropyrolysis of maple wood at varying catalyst:biomass. Shows plots for 0-4O containing species. Reaction conditions: 400-600°C sandbath, 270 psi, 300 mL/min H2, 30 mg biomass, 300 mg passivated NiMo

3.4. Conclusions

This study centers on the elucidation of biomass hydropyrolysis and hydrodeoxygenation chemistry of $NiMoS_x$ catalysts. Heating rates of at least 9.7°C/s during the hydropyrolysis of biomass between the temperatures of 200-400°C using a novel semi-batch reactor. A fast-heating rate, short gas residence times, and close catalyst contact are critical to studying hydropyrolysis at technology-relevant conditions. A total carbon balance of >86% was achieved for cellulose, lignin, and whole biomass hydropyrolysis.

Hydropyrolysis of cellulose largely produced gasoline range products (38.5%), with a majority of the products containing 1-7 carbon atoms. Lignin hydropyrolysis largely produced jet/diesel range products (36.0%) due to a C12+ yield as high as 21.2%. Whole biomass hydropyrolysis produced light gases (28.0%), gasoline range products (23.8%), and jet/diesel range products (10.6%). The hydropyrolysis of whole biomass produced more light gases than expected from the sum of its cellulose and lignin components. This may be due to the mineral content contained in the whole biomass resulting in higher C-C cleavage catalyzed by acid sites.[84-85] Yields of thermocatalytic biomass conversion technologies have been shown to differ from the sum of their cellulose, lignin, and hemicellulose components.[78-79] $NiMoS_x$ catalyst improved the total carbon yield of products from the hydropyrolysis of whole biomass, lignin, and cellulose with increasing catalyst:biomass ratio from 5:1-20:1. The increase in catalyst amount also resulted in higher C-C bond cleavage, producing more light gases. Hydropyrolysis of lignin yielded 3.2%, 21.2%, and 15.1% high boiling species at 5:1, 10:1, and 20:1 catalyst:biomass ratio, respectively. Whole biomass hydropyrolysis yields 9.6% high boiling species at 5:1 catalyst:biomass ratio reducing to 2.3% at 20:1 catalyst:biomass ratio. Whole boiling species may form pyrolytic lignin through oligomerization reactions, resulting in much lower overall yields from lignin hydropyrolysis with low catalyst loading.[11,86] Another possibility for the low overall yields of lignin hydropyrolysis may be due to insufficient capture of the very heavy species. With an increase in catalyst loading, the average molecular weight of the products decreases resulting in a higher observed carbon balance. This is supported by the similar yields of solids during hydropyrolysis at varying catalyst:biomass ratios, indicating the solid yields are a result of pyrolysis instead of secondary reactions. Hydropyrolysis of whole biomass with the sand-bath at 400°C results in substantially lower liquid product yields

and higher solid yields. Changing the sand-bath temperature changes the average pyrolysis temperature, heating rate, and reaction temperature. Low temperature and low heating rate pyrolysis will result in high solid and gas yields.[6,58,87] The yields from biomass hydropyrolysis at 500°C and 600°C are similar, with an increase in gas products and decrease in solid yields with an increase in temperature. The similar yields indicate the heating rate and reaction temperature while at 500°C is sufficient. FTICR-MS of the liquid products qualitatively reveals the functionality of the heavy products from maple wood and lignin. As expected, products from cellulose hydropyrolysis did not contain large oligomers. FTICR-MS data shows mainly dimer species from lignin hydropyrolysis while the products from whole biomass contained trimer species. Dimer and trimer species are mainly composed of non-oxygenated or single-oxygenated compounds. Dimer and trimer species include highly saturated species with an average of 2 DBE per monomer. Unsaturated compounds with a DBE ranging from 8-12 are only present as non-oxygenated hydrocarbon species. This indicates the hydrodeoxygenation pathway of the polyphenols is ring hydrogenation followed by hydrodeoxygenation. The only observed trimer species are highly saturated. Further analysis with more concentrated samples and a wider carbon number range would be required for future investigation.

4. Future Work

4.1. Future direction

This study aims to provide key insight into the complicated reaction pathways of hydrodeoxygenation and hydropyrolysis of poly-oxygenates. The novel reactor designed and built for this project provides a relatively high carbon balance of hydropyrolysis products.[31,58,88] Key reaction conditions such as heating rate, gas residence time, and close catalyst contact were carefully considered to effectively model fluidized bed hydropyrolysis chemistry with a small analytical reactor. To effectively elucidate the hydropyrolysis chemistry, both model compound hydrodeoxygenation and whole biomass hydropyrolysis should be explored.

Model compound hydrodeoxygenation has been investigated throughout many studies, but there are limited studies exploring hydrodeoxygenation at hydropyrolysis conditions with compounds with similar thermal stability. Glycerol HDO provided a chemically similar model for cellulose hydropyrolysis. Glycerol has a similar effective C:H ratio to cellulose, meaning the thermal stability of the compound during pyrolysis is similar to cellulose. Model compounds chemically similar to lignin are more challenging to utilize. Simple model compounds such as phenol, guaiacol, or 4-propyl-guaiacol are helpful to understand hydrodeoxygenation of aromatic hydroxyl group, but have a different C:H effective ratio than lignin with different thermal stability.[15] Hydrodeoxygenation of lignin model compounds containing β-O-4 linkages or compounds resembling reactive monomers, such as coniferyl alcohol, could be helpful to better understand lignin hydropyrolysis. Hydropyrolysis may on various lignin types containing different amounts of β-O-4 ether linkages and C-C linkages.

Hydrodeoxygenation of lignin model compounds containing β-O-4 linkages or compounds resembling reactive monomers, such as coniferyl alcohol, will be performed to compliment the hydropyrolysis work. Lignocellulosic biomass varies mainly in lignin-cellulose-hemicellulose composition, lignin structure, and extractives content. These differences in biomass structure affect the reaction chemistry and ultimately the product distribution. Ether linkages such as β-O-4 linkages in lignin are common in most lignocellulosic biomass but are also generally easy to break thermally and catalytically. Other C-C linkages may be more challenging to break, resulting in more C20+ species. Biomass with higher lignin content could result in a more favorable distillate fuel fraction.

The work comprising this thesis is mainly focused on studying the reaction chemistry rather than exploring catalyst options. Based on the high C-C cleavage activity of $NiMoS_x$ catalysts, new Nickel based catalysts may be investigated for biomass hydropyrolysis. Further catalyst characterization is necessary to better understand the catalytic reaction pathway as well as the deactivation of sulfided catalysts during hydropyrolysis and hydrodeoxygenation reactions. Catalyst characterization of fresh and spent sulfided catalysts typically requires in-situ or operando experiments. Studying the active sites of a sulfided catalyst during hydrodesulfiding (HDS) is challenging but has been extensively studied mainly using XAS characterization.[36,39,89] HDO over a sulfided catalyst is more complicated, especially while co-feeding a Sulphur containing compound such as H_2S or DMDS. Some preliminary studies have been attempted regarding the change in active sites during HDO over a sulfided catalyst, but the studies are limited at pyrolysis temperatures.[37,42,90] XAS studies while the catalyst is in a sulfided state would require in-situ analysis under H_2S pressure. To study the effect of oxygenated compounds, the experiments would likely need to be run operando.

The semi-batch reactor utilized for these experiments was successful at operating hydropyrolysis reactions at conditions like the IH2 process while maintaining high carbon balances.[30] However, there are significant limitations with this reactor design for hydropyrolysis experiments:

- The size of the system limited experiments to biomass samples between 10-50 mg. This resulted in dilute liquid and gas samples, making precise characterization of heavier compounds challenging.
- Temperature of the catalyst is equal to the temperature of the biomass during the experiment. Due to the high heating rate (>10°C/s) and low gas residence times (< 1s), the temperature at which a pyrolytic vapor is formed will be the temperature at which that vapor contacts the catalyst.
- The product recovery and analytical methods utilized enabled the observation of products in the trimer range but may be limited for collection and identification of heavier or more oxygenated species.

4.2. Outlook of biomass hydropyrolysis technologies compared to other renewable catalytic pyrolysis technologies

Catalytic pyrolysis offers key advantages over non-catalytic pyrolysis technologies for both biomass and plastic conversion[22,91]. The catalyst, feedstock, and process conditions significantly affect the economic and sustainable viability of a catalytic pyrolysis technology. Hydropyrolysis of biomass allows for effective heteroatom (O,N,S) removal, low coke yields, and a high overall hydrocarbon yield of 20-30 wt%.[27-28,31] These benefits are contrasted by significant process challenges such as the high total pressure and high hydrogen partial

pressure required. While 10-20 bar is not a high pressure for PFR processes, this is a significant disadvantage for circulating fluidized bed reactor technologies.[52-53] This is mainly due to the high requirement of gas for fluidization and solids transport. Since Hydrogen is an exceedingly poor fluidization gas, this requires a substantial amount of Nitrogen or recycled paraffins for fluidization. Considering continuous catalyst regeneration is necessary for all catalytic pyrolysis technologies, this also means the regenerator must be run at a high pressure as well. The IH2 process boasts the potential for full heat and Hydrogen integration, requiring significant coke burning, light gas reformation, and a reduction in high value carbon products.[27,64] The use of sulfided catalysts for hydrodeoxygenation and hydropyrolysis technologies has been an research topic of interest for the past 15 years. Utilizing sulfided catalysts for these applications results in high deoxygenation, but also high C-C cleavage, poor aromatization/C-C coupling activity, requiring the use of a sulfur co-feed, introducing a negative impurity into your feedstock.[11,37,40,71,92] Molybdenum sulfide catalysts are utilized to great success in petroleum processing, where petroleum feedstocks contain a significant amount more sulfur and far less oxygen than biomass. If catalyst deactivation can be significantly limited, these catalysts may be successfully utilized for hydrodeoxygenation applications. Since coke burning must be done continuously, increasing the complexity of the process due to the separate coke burning and sulfiding required for regeneration. Zeolite catalysts offer a significant advantage over base metal catalysts, especially sulfided catalysts.[16,93-94] This is mostly because of the high aromatization activity for olefins and aldehydes to single aromatics and polyaromatics. The major limitation of biomass pyrolysis over a zeolite catalyst is the high yields (>25 wt%) of CO_x, which have limited value as a product. The high CO_x yield is a result of the poor hydrogenation activity in a zeolite, limiting

oxygen removal as water. The biggest limitation to biomass conversion to carbon-rich liquid fuels is the nearly 50 wt% oxygen content. Waste plastics range in composition of Oxygen, Nitrogen, and Halogen content, but an average consumer waste stream will typically have over 80 wt% Carbon.[95-98] This reveals an opportunity for renewable carbon-based liquid fuels and commodity chemical production. The upstream solids processing for biomass and plastics is a significant challenge and impacts both feedstocks economic and sustainable viability. Ultimately combating climate change requires a multi-pronged approach, leaving room for many technologies and alternative feedstocks.

5. References

[1] G. W. Huber, a. Sara Iborra, A. Corma*, **2006**.

[2] D. Gielen, F. Boshell, D. Saygin, M. D. Bazilian, N. Wagner, R. Gorini, *Energy Strategy Reviews* **2019**, *24*, 38-50.

[3] H. K. Jeswani, A. Chilvers, A. Azapagic, *Proceedings of the Royal Society A* **2020**, *476*, 20200351.

[4] D. M. Alonso, J. Q. Bond, J. A. Dumesic, *Green chemistry* **2010**, *12*, 1493-1513.

[5] R. Vanholme, B. Demedts, K. Morreel, J. Ralph, W. Boerjan, *Plant physiology* **2010**, *153*, 895-905.

[6] D. Mohan, C. U. Pittman, P. H. Steele.

[7] E. Gnansounou, A. Dauriat, *Bioresource technology* **2010**, *101*, 4980-4991.

[8] T. D. Foust, A. Aden, A. Dutta, S. Phillips, *Cellulose* **2009**, *16*, 547-565.

[9] *Fuel* **2007**, *86*, 1781-1788.

[10] Dinesh Mohan, †,‡, J. Charles U. Pittman, † and, P. H. Steele§, **2006**.

[11] K. Routray, K. J. Barnett, G. W. Huber, *Energy Technology* **2017**, *5*, 80-93.

[12] T. R. Carlson, Y.-T. Cheng, J. Jae, G. W. Huber, *Energy Environ. Sci.* **2011**, *4*, 145-161.

[13] T. R. Carlson, G. A. Tompsett, W. C. Conner, G. W. Huber, *Topics in Catalysis* **2009**, *52*, 241-252.

[14] F. L. P. Resende, *Catalysis Today* **2016**, *269*, 148-155.

[15] H. Zhang, Y.-T. Cheng, T. P. Vispute, R. Xiao, G. W. Huber, *Energy & Environmental Science* **2011**, *4*, 2297-2307.

[16] J. Liang, G. Shan, Y. Sun, *Renewable and Sustainable Energy Reviews* **2021**, *139*, 110707.

[17] B. Donnis, R. G. Egeberg, P. Blom, K. G. Knudsen, *Topics in Catalysis* **2009**, *52*, 229-240.

[18] A. H. Zacher, M. V. Olarte, D. M. Santosa, D. C. Elliott, S. B. Jones, *Green Chem.* **2014**, *16*, 491-515.

[19] D. C. Elliott, T. R. Hart, G. G. Neuenschwander, L. J. Rotness, M. V. Olarte, A. H. Zacher, Y. Solantausta, *Energy & Fuels* **2012**, *26*, 3891-3896.

[20] R. J. French, J. Stunkel, R. M. Baldwin, *Energy & Fuels* **2011**, *25*, 3266-3274.

[21] H. Wang, J. Male, Y. Wang, *ACS Catalysis* **2013**, *3*, 1047-1070.

[22] D. C. Elliott, *Current Opinion in Chemical Engineering* **2015**, *9*, 59-65.

[23] D. A. Laird, R. C. Brown, J. E. Amonette, J. Lehmann, *Biofuels, bioproducts and biorefining* **2009**, *3*, 547-562.

[24] X. Zhang, T. Wang, L. Ma, Q. Zhang, T. Jiang, *Bioresource technology* **2013**, *127*, 306-311.

[25] K. Wang, K. H. Kim, R. C. Brown, *Green Chemistry* **2014**, *16*, 727-735.

[26] R. Pindoria, A. Megaritis, A. Herod, R. Kandiyoti, *Fuel* **1998**, *77*, 1715-1726.

[27] T. L. Marker, L. G. Felix, M. B. Linck, M. J. Roberts, *Environmental Progress & Sustainable Energy* **2012**, *31*, 191-199.

[28] T. L. Marker, L. G. Felix, M. B. Linck, M. J. Roberts, P. Ortiz-Toral, J. Wangerow, *Environmental Progress & Sustainable Energy* **2014**, *33*, 762-768.

[29] G. Perkins, T. Bhaskar, M. Konarova, *Renewable and Sustainable Energy Reviews* **2018**, *90*, 292-315.

[30] T. L. Marker, G. T. I. D. P. IL, L. G. Felix, G. T. I. B. AL, M. B. Linck, G. T. I. D. P. IL, M. J. Roberts, G. T. I. D. P. IL, P. Ortiz-Toral, G. T. I. D. P. IL, J. Wangerow, G. T. I. D. P. IL, *Environmental Progress & Sustainable Energy* **2018**, *33*, 762-768.

[31] D. C. Dayton, J. Hlebak, J. R. Carpenter, K. Wang, O. D. Mante, J. E. Peters, *Energy & Fuels* **2016**, *30*, 4879-4887.
[32] D. C. Dayton, J. Carpenter, J. Farmer, B. Turk, R. Gupta, *Energy & Fuels* **2013**, *27*, 3778-3785.
[33] M. Z. Stummann, M. Høj, C. B. Schandel, A. B. Hansen, P. Wiwel, J. Gabrielsen, P. A. Jensen, A. D. Jensen, *Biomass and Bioenergy* **2018**, *115*, 97-107.
[34] M. Z. Stummann, A. B. Hansen, L. P. Hansen, B. Davidsen, S. B. Rasmussen, P. Wiwel, J. Gabrielsen, P. A. Jensen, A. D. Jensen, M. Høj, *Energy & fuels* **2019**, *33*, 1302-1313.
[35] S. Kasiraju, L. Grabow, *AIChE Journal* **2018**.
[36] N.-Y. Topsøe, H. Topsøe, *Journal of Catalysis* **1983**, *84*, 386-401.
[37] T. M. H. Dabros, A. Gaur, D. G. Pintos, P. Sprenger, M. Høj, T. W. Hansen, F. Studt, J. Gabrielsen, J.-D. Grunwaldt, A. D. Jensen, *Applied Catalysis A: General* **2018**, *551*, 106-121.
[38] H. Topsøe, B. S. Clausen, F. E. Massoth, in *Catalysis*, Springer, **1996**, pp. 1-269.
[39] E. Laurent, B. Delmon, *Journal of Catalysis* **1994**, *146*, 281-291.
[40] R. Resources, **2013**.
[41] Q. Bu, H. Lei, A. H. Zacher, L. Wang, S. Ren, J. Liang, Y. Wei, Y. Liu, J. Tang, Q. Zhang, R. Ruan, *Bioresource Technology* **2012**, *124*, 470-477.
[42] A. L. Jongerius, R. Jastrzebski, P. C. A. Bruijnincx, B. M. Weckhuysen, *Journal of Catalysis* **2012**, *285*, 315-323.
[43] T. M. H. Dabros, **2017**.
[44] I. D. Mora-Vergara, L. Hernández Moscoso, E. M. Gaigneaux, S. A. Giraldo, V. G. Baldovino-Medrano, *Catalysis Today* **2018**, *302*, 125-135.
[45] A. Gutierrez, E.-M. Turpeinen, T.-R. Viljava, O. Krause, *Catalysis Today* **2017**, *285*, 125-134.
[46] N. Chen, T. Degnan, L. Koenig, *Chemtech* **1986**, *16*, 506-511.
[47] T. R. Carlson, G. A. Tompsett, W. C. Conner, G. W. Huber, *Topics in Catalysis* **2009**, *52*, 241-252.
[48] D. P. Gamliel, G. M. Bollas, J. A. Valla, *Fuel* **2018**, *216*, 160-170.
[49] T. M. Dabros, M. Z. Stummann, M. Høj, P. A. Jensen, J.-D. Grunwaldt, J. Gabrielsen, P. M. Mortensen, A. D. Jensen, *Progress in Energy and Combustion Science* **2018**, *68*, 268-309.
[50] T. Li, J. Su, H. Wang, C. Wang, W. Xie, K. Wang, *Applied Energy* **2022**, *316*, 119115.
[51] Y. He, Y. Zhao, M. Chai, Z. Zhou, M. Sarker, C. Li, R. Liu, J. Cai, X. Liu, *Renewable and Sustainable Energy Reviews* **2020**, *119*, 109604.
[52] N. Couto, V. Silva, C. Bispo, A. Rouboa, *Energy Conversion and Management* **2016**, *119*, 177-186.
[53] J. M. Matsen, *Powder Technology* **1996**, *88*, 237-244.
[54] M. Z. Stummann, M. Høj, B. Davidsen, L. P. Hansen, P. Beato, J. Gabrielsen, P. A. Jensen, A. D. Jensen, *Energy & Fuels* **2019**, *33*, 12387-12402.
[55] M. Z. Stummann, M. Høj, A. B. Hansen, P. Beato, P. Wiwel, J. Gabrielsen, P. A. Jensen, A. D. Jensen, *Energy & Fuels* **2019**, *33*, 12374-12386.
[56] M. Z. Stummann, M. Høj, A. B. Hansen, B. Davidsen, P. Wiwel, J. Gabrielsen, P. A. Jensen, A. D. Jensen, *Fuel Processing Technology* **2019**, *193*, 392-403.
[57] M. Z. Stummann, M. Høj, J. Gabrielsen, L. R. Clausen, P. A. Jensen, A. D. Jensen, *Renewable and Sustainable Energy Reviews* **2021**, *143*, 110960.
[58] S. Thangalazhy-Gopakumar, S. Adhikari, R. B. Gupta, S. D. Fernando, *Energy & Fuels* **2011**, *25*, 1191-1199.
[59] O. Jan, R. Marchand, L. C. Anjos, G. V. Seufitelli, E. Nikolla, F. L. Resende, *Energy & Fuels* **2015**, *29*, 1793-1800.

[60] T. R. Carlson, T. P. Vispute, G. W. Huber, *ChemSusChem* **2008**, *1*, 397-400.
[61] F. Melligan, M. Hayes, W. Kwapinski, J. Leahy, *Energy & fuels* **2012**, *26*, 6080-6090.
[62] F. Melligan, M. Hayes, W. Kwapinski, J. Leahy, *Journal of analytical and applied pyrolysis* **2013**, *103*, 369-377.
[63] A. D. Anderson, M. P. Lanci, J. S. Buchanan, J. A. Dumesic, G. W. Huber, *ChemCatChem* **2021**, *13*, 425-437.
[64] T. L. Marker, D. P. GTI (Gas Technology Institute), Illinois 60018, D. P. GTI (Gas Technology Institute), Illinois 60018, L. G. Felix, B. Gas Technology Institute, AL 35203-1821, M. B. Linck, D. P. GTI (Gas Technology Institute), Illinois 60018, M. J. Roberts, D. P. GTI (Gas Technology Institute), Illinois 60018, *Environmental Progress & Sustainable Energy* **2018**, *31*, 191-199.
[65] J. T. Scanlon, D. E. Willis, *Journal of Chromatographic Science* **1985**, *23*, 333-340.
[66] P. J. Dietrich, R. J. Lobo-Lapidus, T. Wu, A. Sumer, M. C. Akatay, B. R. Fingland, N. Guo, J. A. Dumesic, C. L. Marshall, E. Stach, *Topics in Catalysis* **2012**, *55*, 53-69.
[67] M. Badawi, J. Paul, S. Cristol, E. Payen, Y. Romero, F. Richard, S. Brunet, D. Lambert, X. Portier, A. Popov, *Journal of catalysis* **2011**, *282*, 155-164.
[68] V. der, D.-C. Arda Ülgen aus Istanbul Berichter, U. F. Wolfgang Hölderich Universitätsprofessor Manfred Martin, **2009**.
[69] Y. Liu, H. Tüysüz, C.-J. Jia, M. Schwickardi, R. Rinaldi, A.-H. Lu, W. Schmidt, F. Schüth, *Chemical Communications* **2010**, *46*, 1238-1240.
[70] G. Sánchez, J. Friggieri, C. Keast, M. Drewery, B. Dlugogorski, E. Kennedy, M. Stockenhuber, *Applied Catalysis B: Environmental* **2014**, *152*, 117-128.
[71] K. A. Johnson, J. B. Powell, J. A. Smegal, Google Patents, **2012**.
[72] C. Mésangeau, S. Yous, B. Pérès, D. Lesieur, T. Besson, *Tetrahedron letters* **2005**, *46*, 2465-2468.
[73] A. Stanislaus, M. Absi-Halabi, K. Al-Dolama, A. Katrib, M. Ismail, *Applied Catalysis* **1988**, *41*, 109-119.
[74] T. M. H. Dabros, M. L. Andersen, S. B. Lindahl, T. W. Hansen, M. Høj, J. Gabrielsen, J.-D. Grunwaldt, A. D. Jensen, *Catalysts* **2019**, *9*, 521.
[75] J. S. Luterbacher, J. M. Rand, D. M. Alonso, J. Han, J. T. Youngquist, C. T. Maravelias, B. F. Pfleger, J. A. Dumesic, *Science* **2014**, *343*, 277-280.
[76] A. Sluiter, B. Hames, R. Ruiz, C. Scarlata, J. Sluiter, D. Templeton, D. Crocker, *Laboratory analytical procedure* **2010**.
[77] Y. Corilo, Florida State University, Omics LLC, Tallahassee, FL, **2014**.
[78] D. J. McClelland, P. H. Galebach, A. H. Motagamwala, A. M. Wittrig, S. D. Karlen, J. S. Buchanan, J. A. Dumesic, G. W. Huber, *Green Chemistry* **2019**, *21*, 2988-3005.
[79] P. H. Galebach, J. K. Soeherman, A. M. Wittrig, M. P. Lanci, G. W. Huber, *ACS Sustainable Chemistry & Engineering* **2019**, *7*, 15361-15372.
[80] Z. J. Brentzel, K. J. Barnett, K. Huang, C. T. Maravelias, J. A. Dumesic, G. W. Huber, *ChemSusChem* **2017**, *10*, 1351-1355.
[81] M. Hronec, K. Fulajtarová, *Catalysis Communications* **2012**, *24*, 100-104.
[82] T. Hosoya, H. Kawamoto, S. Saka, *Journal of Analytical and Applied Pyrolysis* **2007**, *80*, 118-125.
[83] H. Yang, R. Yan, H. Chen, D. H. Lee, C. Zheng, *Fuel* **2007**, *86*, 1781-1788.
[84] P. R. Patwardhan, J. A. Satrio, R. C. Brown, B. H. Shanks, *Bioresource Technology* **2010**, *101*, 4646-4655.
[85] A. K. Burnham, X. Zhou, L. J. Broadbelt.

[86] F.-X. Collard, J. Blin, **2014**.
[87] E. Cetin, B. Moghtaderi, *Fuel* **2005**, *84*, 1328-1334.
[88] V. K. Venkatakrishnan, J. C. Degenstein, A. D. Smeltz, W. N. Delgass, R. Agrawal, F. H. Ribeiro, *Green Chemistry* **2014**, *16*, 792.
[89] A. Travert, †, C. Dujardin, ‡, F. Maugé, E. Veilly, S. Cristol, a. J.-F. Paul, E. Payen‡, **2005**.
[90] X. Wang, R. Y. Saleh, U. S. Ozkan, *Applied Catalysis A: General* **2005**, *286*, 111-119.
[91] T. V. Choudhary, C. B. Phillips, *Applied Catalysis A: General* **2011**, *397*, 1-12.
[92] L. Kaluža, D. Kubička, *Reaction Kinetics, Mechanisms and Catalysis* **2017**, *122*, 333-341.
[93] T. R. Carlson, T. P. Vispute, G. W. Huber.
[94] R. Sotelo-Boyás, Y. Liu, T. Minowa, *Industrial & Engineering Chemistry Research* **2011**, *50*, 2791-2799.
[95] M. Kusenberg, A. Eschenbacher, M. R. Djokic, A. Zayoud, K. Ragaert, S. De Meester, K. M. Van Geem, *Waste Management* **2022**, *138*, 83-115.
[96] S. Nanda, F. Berruti, *Environmental Chemistry Letters* **2021**, *19*, 123-148.
[97] M. S. Qureshi, A. Oasmaa, H. Pihkola, I. Deviatkin, A. Tenhunen, J. Mannila, H. Minkkinen, M. Pohjakallio, J. Laine-Ylijoki, *Journal of Analytical and Applied Pyrolysis* **2020**, *152*, 104804.
[98] D. Sudolsky, *Industrial Biotechnology* **2019**, *15*, 330-333.